Korean J. Chem. Eng., 40(3), 555-571 (2023)
DOI: 10.1007/s11814-022-1352-4

pISSN: 0256-1115
eISSN: 1975-7220

Discontinuous Galerkin finite element scheme for solving non-linear lumped kinetic model of non-isothermal reactive liquid chromatography

Shireen Zafar*, Sadia Perveen,†, and Shamsul Qamar***

*Department of Mathematics, COMSATS University, Park Road, Chak Shahzad, 45550, Islamabad, Pakistan
**Air University, PAF Complex, Sector E-9, 44230, Islamabad, Pakistan
(*Received 19 January 2022 • Revised 26 October 2022 • Accepted 16 November 2022*)

Abstract−A multi-component lumped kinetic model of non-isothermal and non-linear reactive liquid chromatography was formulated and approximated numerically to demonstrate thermal effects on reaction kinetics, adsorption equilibria, and conversion-separation studies in thermally insulated, packed bed, chromatographic reactors. The considered model is constituted of systems of non-linear convection diffusion reaction partial differential equations for mass and energy balances in the bulk phase coupled with differential equations for mass and energy balances in the stationary phase. In this work, a total variation bounded (TVB) Runge-Kutta local-projection discontinuous Galerkin finite element method (DG-FEM) was derived and proposed for the numerical solutions of the model equations. The developed numerical method is robust, explicit, capable of resolving sharp discontinuities and is second-order accurate. System parametric studies treating heterogeneously catalyzed reversible reactions were performed through numerical simulations. The coupling between thermal and concentration fronts, the influence of temperature on reactor efficiency, and the conversion-separation of products are demonstrated through several consistency tests. The results, which authenticate the accuracy of the (DG-FEM) method, will be beneficial for interpreting mass and energy profiles in non-equilibrium and non-isothermal liquid chromatographic reactors and provide deeper insight into the sensitivity of the conversion-separation process.

Keywords: Discontinuous Galerkin Method, Non-isothermal Chromatography, Numerical Simulation, Nonlinear Isotherm, Non-equilibrium Model, Mass and Heat Transfer

INTRODUCTION

The evolving nature of the chemical industry implies a transformation of the traditional vision of chemical engineering, primarily designed for the conversion of raw materials into products through reactions and separations, into a more detailed vision by involving molecular materials, process, and product engineering in interaction with energy, the market, and the environment. A novel combination of technology and science in a sustainable way is required to explore new methods for the development of new processes and products. This can be accomplished through reactive separation processes, such as reactive distillation, reactive crystallization, reactive absorption, reactive extraction, reactive membrane separation, and reactive chromatography [1].

Reactive separations are integrated processes that combine biochemical or chemical reactions and adsorptive separation into a single unit operation. The aim of the method is to increase productivity, improve selectivity, eliminate the need for solvents, reduce the use of energy and, hence, lead to high efficiency intensified systems. Within a chromatographic reactor, the reaction occurs inside the chromatographic column, which is catalyzed by a catalytic adsorbent and has different affinities towards the products and reactants. The technology of reactive chromatography has attracted substantial interest during recent years in the chemical engineering industry and research. This approach is primarily advantageous for equilibrium limited reactions where the simultaneous separation of reaction products, shifts the equilibrium in order to reduce the formation of by-products and to enhance conversion [2]. Reactive chromatography has a wide range of applications, like esterification reactions [3], transesterification [4], alkylations [5], reactions involving sugar [6,7], as well as (de-)hydrogenation [8].

In a simultaneous reaction-separation process, a reaction can occur either in the solid phase or the liquid phase or in both phases. The resulting chromatographic reactor is known as either heterogeneously catalyzed or homogeneously catalyzed or both types of catalyzed reactor. In the case of a homogeneously catalyzed reaction, the separation of catalyst at the column outlet must be considered. Whereas this is not the problem for heterogeneously catalyzed reactions. The main advantage of using a heterogeneous catalyst is the relative ease of catalyst separation from the product stream that aids in the creation of continuous chemical processes. Additionally, heterogeneous catalysts are typically more tolerant. The appropriate choice of catalyst can also influence selectivity and reactor yield. In the present study, we only considered the reversible reaction of type $R \rightleftharpoons P_1+P_2$ in a heterogeneously catalyzed chromatographic reactor. The principle of the chromatographic batch reactor can be easily explained for a reaction of type $R \rightleftharpoons P_1+P_2$. The reactant R is injected in the form of a rectangular plus into the column packed with a solid stationary phase having catalytic properties. The products P_1 and P_2 are produced and separated from the reaction medium

†To whom correspondence should be addressed.
E-mail: sadia.ahsan@mail.au.edu.pk

due to the catalytic nature of the stationary phase. The elution order of the components and the type of reaction have a strong influence on the process of reactive chromatography. To get maximum conversion, it is better for the reactant to travel between the products, resulting in enhanced forward and suppressed backward reactions. For sufficiently long enough column, complete conversion of reactant R into products P_1 and P_2 can be achieved [9]. Practical applications for this type of reaction are ester hydrolysis reactions, which are performed with water in exsess as solvent [10].

High-temperature liquid chromatography (HTLC) has garnered great attention in the chromatographic community in recent years, though its full potential has not yet been recognized. Variation in temperature has a significant impact on the liquid chromatographic process and can be generated either internally or externally [11]. Variations in temperature are mostly carried out to enhance column efficiency, to control the transport speed of components, to decrease or increase the analysis time as per requirement, to amplify the rate of conversion of reactant into product in the case of reactive liquid chromatography, and to improve the separation of components. Although variation in temperature has been often neglected in previous studies while analyzing liquid chromatographic process by assuming the influence of enthalpies of reaction and adsorption as insignificant [12]. The authors in [13-16] have stated that the chromatographic process will deviate from isothermal behavior if the heat of adsorption is considerably high. The primary objective of utilizing temperature as a key parameter for all chromatographers is to minimize the processing time and maximize the separation resolution, which depends on selectivity, consistency and effectiveness as reported in [17-24]. Experimental studies for exothermic esterification reactions catalyzed by an acidic ion-exchange resin considering a reversible reaction of the form $A \rightleftharpoons B+C$ are reported in [14]. Several more studies on non-isothermal liquid chromatography are available in [25-31].

Over the last decades, mathematical modeling has significantly contributed to the advancement of reactive liquid chromatography. This approach has now become an essential part of chemical engineering due to its employment for designing, controlling, and optimizing system behavior. A number of models are available in the literature for understanding the dynamical conduct of transport mechanisms involved in the chromatography process. In general, the models of reactive liquid chromatography involve the effects of dispersion, convection, transfer of heat and mass between the bulk phase and boundary layer, surface diffusion within particles, diffusion within particle pores, heterogeneous reaction at the surface of a catalyst or homogeneous reaction in the liquid phase and adsorption kinetics. Their mathematical representations are achieved with the consideration of some or all of these phenomena, which give rise to a variety of models having different levels of complexity [32-38]. Several models currently exist, some of which are the reactive equilibrium dispersive model (REDM), the reactive general rate model (RGRM), the reactive ideal model (RID), the reactive linear driving force model, and the reactive lumped kinetic model (RLKM).

A number of shock-capturing high-order numerical methods within the total variation diminishing (TVD) framework have been developed in the literature for the approximation of chromatographic models. These numerical techniques are designed to achieve stable solution profiles even in the presence of discontinuities [39-52]. Authors in [53-55] have compared the high-resolution finite volume (FV) schemes over a wide selection of Sweby-type [56] flux limiters and concluded that the Koren scheme [57] is high order accurate and robust in resolving sharp discontinuities. The authors in [58] implemented the weighted essentially non-oscillatory (WENO) finite volume method [59,60] based on the essentially non-oscillatory (ENO) method [61] to simulate multi-component (GRM). An application of the space-time conservation element and solution element (CE/SE) method for solving partial differential algebraic equations (PDAEs) for the illustration of chromatographic adsorption problems including convection, diffusion, and reaction terms with a linear or nonlinear adsorption isotherm is addressed in [62]. In [63], particle transport method (PTM) based on the operator-splitting approach, in combination with the Lagrangian method of characteristics and the method of lines, is applied to simulate nonlinear multi-component chromatography problems. The discontinuous Galerkin finite element method (DG-FEM) was introduced into chromatographic literature by the authors in [64] for solving isothermal non-reactive and reactive (EDM) of liquid chromatography. Later, the use of continuous Galerkin finite element method along with spectral filtering techniques was demonstrated in [65] and a nodal high-order (DG-FEM) is presented in [66] for simulating linear and non-linear liquid chromatography problem described by (EDM). Recently, the total variation bounded (TVB) Runge-Kutta local-projection discontinuous Galerkin (RK-LDG) finite element method was applied for approximating the non-reactive, isothermal [67] and non-isothermal [68,69], non-equilibrium model of liquid chromatography under non-linear adsorption conditions.

In this article, a non-linear, non-isothermal, and reactive non-equilibrium RLKM is approximated numerically using the DG-FEM finite element scheme. This article extends the study of a non-reactive, three-component, non-isothermal, and nonlinear LKM considered in [68] to a reactive, three-component, non-isothermal, and non-linear LKM. Here the reversible reaction of the type $R \rightleftharpoons P_1+P_2$ is considered. The model constitutes a system of PDAEs, including convection, diffusion, reaction terms coupled with non-linear adsorption isotherm. The DG-FEM finite element method is applied and extended to solve the model equations. The second order accuracy of DG-FEM scheme has been verified numerically in [69]. Moreover, the selected second order Runge-Kutta method for the time discretization and the considered flux-limiting function for calculating fluxes at the cell interfaces guarantee the second-order accuracy of the scheme. The main objectives of this research work include (i) the study of non-isothermal and non-equilibrium, reactive liquid chromatography processes considering Langmuir isotherms, and (ii) the formulation of DG-FEM scheme for solution of RLKM. Several case studies of practical relevance were conducted to study the coupling between thermal and concentration fronts in the reaction-separation process. As chromatographic reactors still lack experimental evidence for the validation of their mathematical models, therefore, integral consistency analysis is introduced in this study to verify the validity of numerical results and the correctness of the model formulations.

Moreover, key thermodynamic parameters, such as mass transfer coefficients, enthalpy of adsorption, enthalpy of reaction, activation energy, the ratio of specific heats, and different sample injection modes that influence the reactor performance are identified.

This article is organized as follows. The non-isothermal RLKM is introduced in Section 2. In Section 3, we formulate the discontinuous Galerkin finite-element method DG-FEM to approximate the non-isothermal RLKM. Section 4 is designated for the validation of numerical results through a consistency test. Numerical case studies on the basis of consistency analysis are reported in Section 5, while research work is concluded in Section 6.

MODEL FORMULATION

The lumped kinetic model integrates the local effects of variation in the concentration of sample components present in the stationary state and the deviation of concentration of each component from their equilibrium state values. When these effects are written as rates, they make up what is called the kinetic equation of the segregation process. Furthermore, external as well as internal resistances offered during mass transport are lumped into a single coefficient for mass transfer, k_i [36]. The non-linear reactive lumped kinetic model considered in this study is based on the following assumptions: (i) The chromatographic bed is homogeneous and made up of the same sized porous particles. (ii) Incompressibility of the mobile phase is assumed. (iii) The chromatographic column is radially homogeneous (iv) No interaction between liquid (or mobile) and solid (or stationary) phases is taking place. (v) Consistency of the axial dispersion coefficient is assumed. (vi) A non-isothermal environment is considered. (vii) Reversible heterogeneous reactions of a catalytic nature occur in the solid phase. The material balance equations for the conservation of mass and energy of a multi-component, non-isothermal, reactive lumped kinetic model (RLKM) are expressed as [36]

$$\frac{\partial c_i}{\partial t}+u\frac{\partial c_i}{\partial z}-D_L\frac{\partial^2 c_i}{\partial z^2}+F\frac{\partial q_i}{\partial t}=0,\qquad i=1, 2, \ldots, N_c \tag{1}$$

$$\frac{\partial q_i}{\partial t}-k_i(q_i^*-q_i)=\nu_i r^{het} \tag{2}$$

$$\frac{\partial T}{\partial t}+u\frac{\partial T}{\partial z}-\frac{\lambda_L}{c_f}\frac{\partial^2 T}{\partial z^2}+F\sum_{j=1}^{N_c}\frac{\Delta H_{A,j}}{c_f}\frac{\partial q_i}{\partial t}+F\frac{c_e}{c_f}\frac{\partial T_S}{\partial t}=0, \tag{3}$$

$$\frac{\partial T_S}{\partial t}+\sum_{j=1}^{N_c}\frac{\Delta H_{A,j}}{c_e}\frac{\partial q_j}{\partial t}-\frac{3h_p}{R_p c_e}(T-T_S)=\frac{(-\Delta H_R)r^{het}}{c_e} \tag{4}$$

In the above equations, $c_i(t, z)$, and $q_i(t, z)$ are the i^{th} component of solute concentrations in liquid and solid phases, respectively; T is the temperature in the bulk phase and T_s is the temperature in the stationary phase; the volume phase ratio is given by $F=\frac{1-\varepsilon}{\varepsilon}$ and symbolizes the external porosity, while the density times specific heat in the solid phase is symbolized by $c_e=\rho^S c_p^S$ and in the liquid phase as $c_f=\rho^L c_p^L$, respectively. Furthermore, u is the constant interstitial velocity, t is the time coordinate, z is the column's axial coordinate, D_L is the axial dispersion, k_i is the mass transfer rate coefficient, λ_L is conductivity coefficient, $\Delta H_{A,i}$ is the adsorption enthalpy of the i^{th} component, $-\Delta H_R$ is the enthalpy of exothermic reaction, r^{het} is the heterogeneous reaction rate, ν_i is the stoichiometric coefficients of i^{th} component of the mixture, R_p is the radius of the solid particle, h_p is the coefficient of heat transfer between solid and liquid phases and N_c is the number of components in the mixture. In general, the stoichiometric coefficient ν_i is negative for reactants and positive for products. The temperature dependent equilibrium adsorbate concentration q_i^* in the liquid and adsorbed phases of the i^{th} component based on classical van't Hoff equation is expressed as [14]:

$$q_i^*=\frac{a_{i,ref}c_i\exp\left(\frac{-\Delta H_{A,j}}{R_g}\left[\frac{1}{T_S}-\frac{1}{T_{ref}}\right]\right)}{1+\sum_{j=1}^{N_c}b_{j,ref}\exp\left(\frac{-\Delta H_{A,j}}{R_g}\left[\frac{1}{T_S}-\frac{1}{T_{ref}}\right]\right)},\qquad i=1, 2, \ldots, N_c, \tag{5}$$

where T_{ref} symbolizes the reference temperature, $a_{i,ref}$ is the i^{th} component Henry's constant at reference temperature, $b_{j,ref}$ is the component-wise nonlinearity coefficient at the reference temperature, and R_g is the universal gas constant.

The reaction can occur either in the solid phase or liquid phase or in both phases. The resulting chromatographic reactor is known as either heterogeneously catalyzed or homogeneously catalyzed or both types of catalyzed reactor. For a homogeneously catalyzed reaction, the separation of catalyst at the column outlet must be considered. Whereas this is not a problem for heterogeneously catalyzed reactions. In the present study, we only consider the heterogeneously catalyzed chromatographic reactor. This can be obtained by amending the packing material of the column to behave like a catalyst and have a versatile affinity range for reactant and products. The reaction rate for the reversible three-component reaction model of the type $R\rightleftharpoons P_1+P_2$ is defined as

$$r^{het}=k^{het}(T_S)\left(q_R-\frac{q_{P_1}q_{P_2}}{K_{eq}^{het}(T_S)}\right). \tag{6}$$

where q_R, q_{P_1}, and q_{P_2} are solid phase concentrations of the reactant R and the products P_1 and P_2 in a reversible reaction, $k^{het}(T_S)$ and $K_{eq}^{het}(T_S)$ are the heterogeneous forward reaction rate and chemical equilibrium constants, respectively. The temperature effects on the chemical reaction rate, $k^{het}(T_S)$, can be expressed as follows by using the Arrhenius equation:

$$k^{het}(T_S)=k^{het}(T_{ref})\exp\left(\frac{-E_{Act}}{R_g}\left(\frac{1}{T_S}-\frac{1}{T_{ref}}\right)\right), \tag{7}$$

where E_{Act} is the activation energy. Moreover, chemical equilibrium constant is expressed as

$$K_{eq}^{het}(T_s)=K_{eq}^{het}(T_{ref})\exp\left(\frac{-\Delta H_R}{R_g}\left(\frac{1}{T_s}-\frac{1}{T_{ref}}\right)\right), \tag{8}$$

The solution of the PDEs system represented by Eqs. (1)-(4) requires a suitable selection of initial and boundary conditions. For a chromatographic reactor to be initially in equilibrium, the following initial conditions are considered:

$$c_i(0, z)=c_{i,init},\ T(0, z)=T_{init},\ q_i(0, z)=q_{i,init}^*,\ T_s(0, z)=T_{init}. \tag{9}$$

Classical Danckwerts boundary conditions are exploited in this study

by considering the injection of a rectangular mixture pulse at the reactor inlet, while zero Neumann boundary conditions are utilized at the reactor outlet:

$$-\frac{D_L}{u}\frac{\partial c_i}{\partial z}(t,0)+c_i(t,0)=\begin{cases} c_{i,inj}, & \text{if } 0\le t\le t_{inj,} \\ 0 & \text{if } t>t_{inj,}\end{cases}, \qquad \frac{\partial c_i(t,L)}{\partial z}=0. \tag{10}$$

To facilitate our analysis, let us introduce the following transformation for the temperature in the liquid and solid phases:

$$c_{N_c+1=T-T_{inj}}, \qquad q_{N_c+1=T_s-T_{inj}}. \tag{11}$$

Moreover, the following dimensionless variables are introduced to reduce the number of variables involved in the model equations and to simplify the notations:

$$\tau=\frac{ut}{L}, \; x=\frac{z}{L}, \; Pe_c=\frac{uL}{D_L}, \; Pe_T=\frac{uLc_f}{\lambda_L},$$
$$H_L=\frac{3h_p}{uR_pc_f}, \; H_S=\frac{3h_pL}{uR_pc_e}, \; \kappa_i=\frac{Lk_i}{u}. \tag{12}$$

Substitution of the above transformations in Eqs. (1)-(4) gives the following system of equations:

$$\frac{\partial c_i}{\partial \tau}+\frac{\partial c_i}{\partial x}-\frac{1}{Pe_n}\frac{\partial^2 c_i}{\partial x^2}+(1-\delta_{im})F\left[\frac{\partial q_i}{\partial \tau}+\frac{L}{u}\nu_i r^{het}\right] + \delta_{im}FH_L(c_m-q_m)=0, \tag{13}$$

$$\frac{\partial q_i}{\partial \tau}-(1-\delta_{im})\left[\kappa_i(q_i^*-q_i)+\frac{L}{u}\nu_i r^{het}\right] + \delta_{im}\left[\sum_{j=1}^{N_c}\frac{\Delta H_{A,j}}{c_e}\frac{\partial q_j}{\partial \tau}-H_S(c_m-q_m)-\frac{L(-\Delta H_R)r^{het}}{uc_e}\right]=0, \tag{14}$$

where, i=1, 2, …, m=N_c+1, δ_{ij} is the Kronecker's delta function, and

$$Pe_n=\begin{cases} Pe_c, & n\le N_c \\ Pe_T, & n=N_c+1\end{cases}. \tag{15}$$

THE DISCONTINUOUS GALERKIN SCHEME

In this section, the proposed discontinuous Galerkin finite element method DG-FEM is extended for solving the non-isothermal RLKM given by Eqs. (13) and (14). For effective presentation and simple explanation of core ideas, the derivation of DG-FEM is presented below for three-component non-isothermal RLKM. The scheme could be extended to multicomponent flows in an analogous manner. In the three-component reaction case (i.e., for N_c=3), Eqs. (13) and (14) reduce to

$$\frac{\partial c_i}{\partial \tau}+\frac{\partial c_i}{\partial x}-\frac{1}{Pe_c}\frac{\partial^2 c_i}{\partial x^2}+F\frac{\partial q_i}{\partial \tau}+F\frac{L}{u}\nu_i r^{het}=0, \tag{16}$$

$$\frac{\partial c_4}{\partial \tau}+\frac{\partial c_4}{\partial x}-\frac{1}{Pe_T}\frac{\partial^2 c_4}{\partial x^2}+FH_L(c_4-q_4)=0, \tag{17}$$

$$\frac{\partial q_i}{\partial \tau}-\kappa_i(q_i^*-q_i)-\frac{L}{u}\nu_i r^{het}=0, \tag{18}$$

$$\frac{\partial q_4}{\partial \tau}+\sum_{i=1}^{3}\frac{\Delta H_{A,i}}{c_e}\frac{\partial q_i}{\partial \tau}-H_S(c_4-q_4)-\frac{L(-\Delta H_R)r^{het}}{uc_e}=0. \tag{19}$$

where, i=1, 2, 3. Introducing the following two flux functions as:

$$g_j(c_j)=\frac{1}{\sqrt{Pe_j}}\frac{\partial c_j}{\partial x}, \; f_j(c_j,g_j)=c_j-\frac{1}{\sqrt{Pe_j}}g_j, \qquad j=1,2,3,4. \tag{20}$$

Then, the PDEs system given in Eqs. (16)-(19) acquire the following forms:

$$\frac{\partial c_i}{\partial \tau}+\frac{\partial f_i}{\partial x}+F\kappa_i(q_i^*-q_i)=0, \tag{21}$$

$$\frac{\partial c_4}{\partial \tau}+\frac{\partial f_4}{\partial x}+FH_L(c_4-q_4)=0, \tag{22}$$

$$g_j=\frac{1}{\sqrt{Pe_j}}\frac{\partial c_j}{\partial x}, \qquad j=1,2,3,4, \tag{23}$$

$$\frac{\partial q_i}{\partial \tau}-\kappa_i(q_i^*-q_i)-\frac{L}{u}\nu_i r^{het}=0, \tag{24}$$

$$\frac{\partial q_4}{\partial \tau}+\sum_{i=1}^{3}\frac{\Delta H_{A,i}}{c_e}\kappa_i(q_i^*-q_i)+\sum_{i=1}^{3}\frac{L(\Delta H_{A,i})\nu_i r^{het}}{uc_e} -H_S(c_4-q_4)-\frac{L(-\Delta H_R)r^{het}}{uc_e}=0. \tag{25}$$

The numerical solution of the model equation Eqs. (1)-(4) is equivalent to the numerical solution of the aforementioned equations Eqs. (21)-(25). The continuous finite element method is not well suited for problems with significant variations in field variables ($c_i(\tau, x)$) across the cell interfaces, because implementing the assumption of continuity across the cell interfaces leads to solutions that do not easily converge to the physical solutions to the mod-

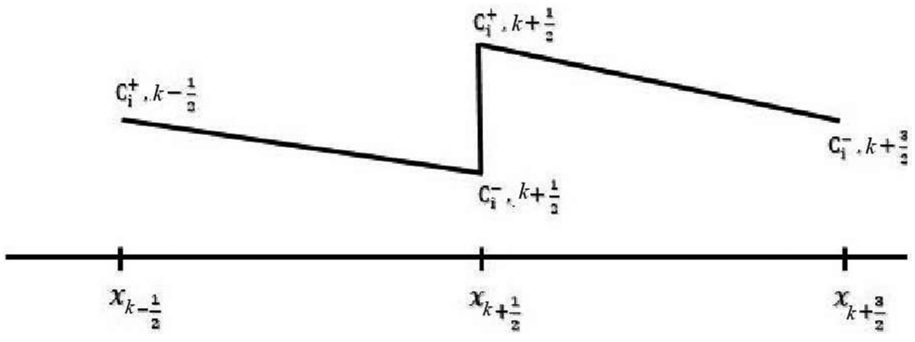

Fig. 1. Illustration of jump discontinuities at the cell interfaces of the domain.

eled problems [70]. The discontinuous Galerkin finite element method, DG-FEM, preserves the property of conservation in the field variable by allowing finite jump discontinuities at the interfaces of the cell (c.f. Fig. 1). The current model forms a system of convection-diffusion-reaction systems of PDEs with convection-dominated terms. The current reaction terms, which act as source terms, are not stiff and the resulting concentration and temperature profiles are found to be smooth enough. Thus, the resulting non-stiff ODE-system was solved efficiently with the considered RK-method. However, if a situation occurs in which the reaction term is much dominated, the implicit ODE-solver can be applied without any difficulty.

1. Spatial Discretization

To formulate DG-FEM scheme, the axial domain ($x\in[0,1]$) is discretized as follows. Let the set $\left\{x_{k+\frac{1}{2}}\right\}_{k=0}^{N}$ partitioned the domain [0,1], in to finite collection of disjoint, open subsets $I_k=\left(x_{k-\frac{1}{2}}, x_{k+\frac{1}{2}}\right)$ such that $I=U_kI_k$ be the partition of the whole domain. The corresponding width of the k^{th} cell is $\Delta x_k=x_{k+\frac{1}{2}}-x_{k-\frac{1}{2}}$; we also denote $h=\sup_k\{\Delta x_k\}$ (c.f. Fig. 1) and $x_k=\frac{1}{2}\left(x_{k+\frac{1}{2}}+x_{k-\frac{1}{2}}\right)$. Here, we assume that mesh partition is equidistant.

2. Solution Approximation

Let V_h be defined as the piece-wise polynomial space on the partition, where $P_M(I_k)$ is the space of polynomial function of degree less than or equal to M and is defined on the cell I_k.

$$V_h=\{u\in L^k(I) : u|_{I_k}\in P_M(I_k),\ k=1, 2, \ldots, N\}, \tag{26}$$

where $L^k(I)$ is a Hilbert space. The approximate solution $(c_i(\tau, x))_h$ to $c_i(\tau, x)$ for each $\tau\in[0, \tau_{max}]$, $(c_i(\tau, x))_h$ belongs to the finite dimensional space V_h, $\tau_{max}=ut_{max}/L$, with t_{max} being the final simulation time. The functions in V_h exhibit element-wise polynomial behavior but may be discontinuous across element interfaces, and thus are allowed to have jumped at the intersection of cell interfaces, i.e., at $x_{k\pm\frac{1}{2}}$.

3. Weak Formulations

The application of DG-FEM scheme needs weak formulations to get the approximate solution $(c_i(\tau, x))_h$ of the model equations. To acquire weak formulation, multiply Eqs. (21)-(25) by an arbitrary smooth test function v(x), integrate the resulting equation over the cell I_k and perform integration by parts to obtain [71]:

$$\int_{I_k}\frac{\partial c_i}{\partial\tau}v(x)dx=-\left(f_i\left(c_{i,k+\frac{1}{2}}, g_{i,k+\frac{1}{2}}\right)v\left(x_{k+\frac{1}{2}}\right)-f_i\left(c_{i,k-\frac{1}{2}}, g_{i,k-\frac{1}{2}}\right)v\left(x_{k-\frac{1}{2}}\right)\right)+\int_{I_k}\left(f_i\frac{\partial v}{\partial x}-F_{\kappa_i}(q_i^*-q_i)v(x)\right)dx, \tag{27}$$

$$\int_{I_k}\frac{\partial c_4}{\partial\tau}v(x)dx=-\left(f_4\left(c_{4,k+\frac{1}{2}}, g_{4,k+\frac{1}{2}}\right)v\left(x_{k+\frac{1}{2}}\right)-f_4\left(c_{4,k-\frac{1}{2}}, g_{4,k-\frac{1}{2}}\right)v\left(x_{k-\frac{1}{2}}\right)\right)+\int_{I_k}\left(f_4\frac{\partial v}{\partial x}-FH_L(c_4-q_4)v(x)\right)dx, \tag{28}$$

$$\int_{I_k}g_jv(x)dx=\frac{1}{\sqrt{Pe_j}}\left\{\left(f_j\left(c_{j,k+\frac{1}{2}}, 0\right)v\left(x_{k+\frac{1}{2}}\right)-f_j\left(c_{j,k-\frac{1}{2}}, 0\right)v\left(x_{k-\frac{1}{2}}\right)\right)-\int_{I_k}f_j(c_j, 0)\frac{\partial v}{\partial x}dx\right\},\quad j=1, 2, 3, 4 \tag{29}$$

$$\int_{I_k}\frac{\partial q_i}{\partial\tau}v(x)dx=\int_{I_k}\kappa_i(q_i^*-q_i)v(x)dx+\frac{L}{u}\int_{I_k}\nu_ir^{het}v(x)dx, \tag{30}$$

$$\int_{I_k}\frac{\partial q_4}{\partial\tau}v(x)dx=-\sum_{i=1}^{3}\frac{\Delta H_{A,i}\kappa_i}{c_e}\int_{I_k}(q_i^*-q_i)v(x)dx-\sum_{i=1}^{3}\frac{\Delta H_{A,i}L}{uc_e}\int_{I_k}\nu_ir^{het}v(x)dx+H_S\int_{I_k}(c_4-q_4)v(x)dx+\frac{L}{uc_e}\int_{I_k}(-\Delta H_R)r^{het}v(x)dx, \tag{31}$$

The weak formulations in Eqs. (27)-(31) must hold for any smooth test function $v(x)\in C^\infty(I_k)$. In these formulations the derivatives are shifted to the smooth test function v(x) from the dependent variables. Numerical solution to Eqs. (1)-(4) is equivalent to the numerical solution of Eqs. (27)-(31), but not necessarily vice versa. The aforementioned weak formulation is the basis for approximations that lead to DG-FEM. It is a fundamental aspect of a class of approximations that are called variational methods.

4. Selection of Appropriate Basis Functions

To implement Eq. (26) by means of Galerkin weak formulations, we chose standardized Legendre polynomials $P_M(x)$ of order M and defined them as local orthogonal basis functions over the domain element I_k. The L^2-orthogonality property of standardized Legendre polynomials was used:

$$\int_{-1}^{1}P_n(s)P_{n'}(s)ds=\frac{2}{2n+1}\delta_{nn'}\quad\text{where}\quad\delta_{nn'}=\begin{cases}1, & \text{if } n=n',\\ 0, & \text{if } n\neq n'.\end{cases} \tag{32}$$

For each the approximate solutions $(c_{i,k})_h$, $(g_{i,k})_h$, and $(q_{i,k})_h$ belong to the finite dimensional space V_h (c.f. Eq. (26)). We chose the local orthogonal basis functions $\{v_l, l=0, 1, 2, \ldots, M\}$, named as the standardized Legendre polynomials P_l, over cell I_k and defined as:

$$v_l(x)=P_l(2(x-x_k)/\Delta x_k),\ l=0, 1, 2, \ldots, M. \tag{33}$$

Then the approximate solutions $(c_{i,k})_h$, $(g_{i,k})_h$, and $(q_{i,k})_h$ can be expressed as a linear combination of the chosen basis function for each $x\in I_k$:

$$(c_{i,k})_h=\sum_{l=0}^{M}c_{i,k}^{l}\nu_l(x),\ (g_{i,k})_h=\sum_{l=0}^{M}G_{i,k}^{l}\nu_l(x),\ (q_{i,k})_h=\sum_{l=0}^{M}q_{i,k}^{l}\nu_l(x), \tag{34}$$

where, linear basis functions were utilized in the present study, hence M=1 and therefore l=0, 1. It can be verified easily by using Eqs. (32)-(34):

$$w_{i,k}^{(l)}(t)=\frac{2l+1}{\Delta x_k}\int_{I_k}(w_{i,k})_h(\tau, x)v_l(x)dx,\ w\in\{c, g, q, q^*\},\quad i=1, 2, 3, 4,\ k=1, 2, \ldots, N. \tag{35}$$

The test function $P_l\in V_h$ replaces the smooth function v(x) and the approximate solutions $(c_i)_h$, $(g_i)_h$ and $(q_i)_h$ replace the exact solutions c_i, g_i, and q_i, respectively, and the space of smooth test functions is reduced to the finite-dimensional polynomial space P. Hence, the equations must hold for all functions in P^2, which is achieved by substituting v with polynomial basis of P. Also, the appropriately selected numerical flux functions that depend on two values of

$(c_i)_h$ at the point of discontinuity can be used to replace the functions $f_i\left(c_{i,\,k\pm\frac{1}{2}},\, g_{i,\,k\pm\frac{1}{2}}\right)$, since the functions $f_i\left(c_{i,\,k\pm\frac{1}{2}},\, g_{i,\,k\pm\frac{1}{2}}\right)$ are not defined at cell interfaces ∂I_k:

$$f_i\left(c_{i,\,k+\frac{1}{2}},\, g_{i,\,k+\frac{1}{2}}\right)\approx h_{i,\,k+\frac{1}{2}}=h_i\left(c^{-}_{k+\frac{1}{2}},\, c^{+}_{k+\frac{1}{2}}\right), \tag{36}$$

where c^{-} and c^{+} are, respectively, the left and right limit of c at the interface. As $g_i := g_i(c_i)$, for simplification, it can be neglected from the arguments of h_i (c.f. Eq. (36)). The weak formulations in Eqs. (27)-(31) take the form of either ODEs or algebraic equations by utilizing the above formulations:

$$\frac{dc^{(l)}_{i,\,k}}{d\tau}=-\frac{2l+1}{\Delta x_k}\left(h_{i,\,k+\frac{1}{2}}v_l\left(x_{k+\frac{1}{2}}\right)-h_{i,\,k-\frac{1}{2}}v_l\left(x_{k-\frac{1}{2}}\right)\right)$$
$$-F_{\kappa_i}(q^{*(l)}_{i,\,k}-q^{(l)}_{i,\,k})+\frac{2l+1}{\Delta x_k}\int_{I_k} f_i\frac{dv_l}{dx}dx, \tag{37}$$

$$\frac{dc^{(l)}_{4,\,k}}{d\tau}=-\frac{2l+1}{\Delta x_k}\left(h_{4,\,k+\frac{1}{2}}v_l\left(x_{k+\frac{1}{2}}\right)-h_{4,\,k-\frac{1}{2}}v_l\left(x_{k-\frac{1}{2}}\right)\right)$$
$$-FH_L(c^{(l)}_{4,\,k}-q^{(l)}_{4,\,k})+\frac{2l+1}{\Delta x_k}\int_{I_k} f_4\frac{dv_l}{dx}dx, \tag{38}$$

$$g^{(l)}_{j,\,k}=\frac{2l+1}{\Delta x_k}\frac{1}{\sqrt{Pe_j}}$$
$$\left\{\left(f_j\left(c_{j,\,k+\frac{1}{2}},\,0\right)v_l\left(x_{k+\frac{1}{2}}\right)-f_j\left(c_{j,\,k-\frac{1}{2}},\,0\right)v_l\left(x_{k-\frac{1}{2}}\right)\right)-\int_{I_k} f_j(c_j,\,0)\frac{dv_l}{dx}\right\}, \tag{39}$$

j=1, 2, 3, 4

$$\frac{dq^{(l)}_{i,\,k}}{d\tau}=\kappa_i(q^{*(l)}_{i,\,k}-q^{(l)}_{i,\,k})+\frac{2l+1}{\Delta x_k}\frac{L}{u}\int_{I_k}\nu_i r^{het}v_l(x)dx, \tag{40}$$

$$\frac{dq^{(l)}_{4,\,k}}{d\tau}=\sum_{i=1}^{3}\frac{\Delta H_{A,\,i}\kappa_i}{c_e}(q^{*(l)}_{i,\,k}-q^{(l)}_{i,\,k})+H_S(c^{(l)}_{4,\,k}-q^{(l)}_{4,\,k})+$$
$$\frac{2l+1}{\Delta x_k}\frac{L}{u}\left(\int_{I_k}\frac{(-\Delta H_R)r^{het}v_l(x)}{c_e}dx-\sum_{i=1}^{3}\frac{(\Delta H_{A,\,i})}{c_e}\int_{I_k}\nu_i r^{het}v_l(x)\right). \tag{41}$$

The initial data in the form of new weak formulations can be expressed as (c.f. Eq. (35))

$$c^{(l)}_{i,\,k}(0)=\frac{2l+1}{\Delta x_k}\int_{I_k} c_i(0,\,x)v_l(x)dx, \tag{42}$$

$$g^{(l)}_{i,\,k}(0)=h(c^{(l)}_{i,\,k}(0)),\ q^{(l)}_{i,\,k}(0)=q(c^{(l)}_{i,\,k}(0)),\ i=1,\,2,\,3,\,4. \tag{43}$$

To calculate the values of fluxes at the cell interface, an accurate numerical flux function h_i is required to be chosen for effective functioning of the current numerical scheme. Accurate numerical results can be achieved by specifying numerical flux function, which is consistent (i.e., $h_i(c_i,\,c_i)=f_i(c_i)$), monotonic and Lipschitz continuous. It means that $h_i(\cdot,\cdot)$ should be increasing in its first argument and decreasing in its second argument [72]. A variety of such numerical flux functions are available in literature [71,73-75]. For the considered convective nature non-isotherm LKM, we have utilized the local monotone Lax-Friedrichs flux as defined below:

$$h^{LLF}_i(a,\,b)=\frac{1}{2}[f_i(a,\,g_i(a))+f_i(b,\,g_i(b))-C(b-a)],$$

where

$$C=\max_{min(a,\,b)\le s\le max(a,\,b)}\left|f'_i(s,\,g_i(s))\right| \tag{44}$$

For the case when f'_i are convex functions, $f''_i>0$ and hence C= max(|f'i(a), |f'i(b)|).

The Gauss-Lobatto quadrature rule of order 10 was used to approximate the integral terms on the right hand side of Eqs. (37)-(41). It is well known that most higher-order methods exhibit oscillatory behavior in their numerical results. To prevent non-physical oscillations, a local projection limiter is used to achieve the total variation stability of the DG-FEM scheme. In this article, limiting procedure is introduced through the modification of interface values $c^{\pm}_{i,\,k\pm\frac{1}{2}}$.

Thus we write

$$\bar{c}_{\,i,\,k+\frac{1}{2}}=c^{(0)}_{i,\,k}+\tilde{c}_{i,\,k},\ \bar{\tilde{c}}_{\,i,\,k-\frac{1}{2}}=c^{(0)}_{i,\,k}-\tilde{\tilde{c}}_{i,\,k}, \tag{45}$$

where,

$$\tilde{c}_{i,\,k}=\sum_{l=1}^{M}c^{(l)}_{i,\,k}\,\nu_l\left(x_{k+\frac{1}{2}}\right),\ \tilde{\tilde{c}}_{i,\,k}=-\sum_{l=1}^{M}(c_{i,\,k})^{(l)}\,\nu_l\left(x_{k-\frac{1}{2}}\right). \tag{46}$$

Van Leer slope Limiters [76,77] are used to modify the relations in Eq. (46), to achieve local positivity, which are defined as

$$\tilde{c}_{i,\,k}=mm(\tilde{c}_{i,\,k},\,\Delta_k+c^{(0)}_{i,\,k},\,\Delta_k+c^{(0)}_{i,\,k})$$
$$\tilde{\tilde{c}}_{i,\,k}=mm(\tilde{\tilde{c}}_{i,\,k},\,\Delta_k+c^{(0)}_{i,\,k},\,\Delta_k+c^{(0)}_{i,\,k}) \tag{47}$$

where, the symbol mm stands for the minmod function and is defined as

$$mm(w_1,\,w_2,\,w_3)$$
$$=\begin{cases}\text{s.}\min\limits_{1\le j\le 3}|w_j|. & \text{if } \text{sign}(w_1)=\text{sign}(w_2)=\text{sign}(w_3)=\text{s},\\ 0, & \text{otherwise.}\end{cases} \tag{48}$$

The usage of a minmod limiter is theoretically only first-order accurate and implements a large numerical dissipation at extrema of the function. In application, however, the overall second-order accuracy of the scheme can still be maintained. Furthermore, high-order accuracy of the scheme can be achieved by utilizing the WENO limiters [59].

Eq. (45) can now be written as

$$\bar{c}^{(mod)}_{\,i,\,k+\frac{1}{2}}=c^{(0)}_{i,\,k}+\tilde{c}_{i,\,k},\ \bar{c}^{(mod)}_{\,i,\,k-\frac{1}{2}}=c^{(0)}_{i,\,k}-\tilde{\tilde{c}}^{(mod)}_{i,\,k}, \tag{49}$$

and Eq. (36) can be modified as

$$h_{\,i,\,k+\frac{1}{2}}=h_i\left(\bar{c}^{(mod)}_{\,i,\,k+\frac{1}{2}},\,\bar{c}^{(mod)}_{\,i,\,k-\frac{1}{2}}\right). \tag{50}$$

The local projection limiter defined in Eqs.(47)-(49) stabilizes the DG-FEM scheme without degrading its order of accuracy, and thus convergence can be achieved without oscillations near shocks. The implementation of weak formulations (c.f. Eqs. (37)-(40))

results in a semi-discrete system of ODEs, that can be written in concise form as

$$\frac{dw_h}{d\tau} = L_h(t, w_h), \tag{51}$$

where, $\mathbf{w}_h=[c_1, c_2, q_1, q_2]^T$. The r^{th}-order TVB RK-method is used to solve the above system of ODEs as follows:

$$\mathbf{w}_h^k = \sum_{l=0}^{k-1} \{ \alpha_{kl}\mathbf{w}_h^{(l)} + \gamma_{kl}\Delta\tau L_h(\mathbf{w}_h^{(l)}, \tau^n + d_l\Delta\tau)\}, \quad k=1, 2, \ldots r, \tag{52}$$

where the initial data in Eq. (43)) can be expressed as

$$\mathbf{w}_h^{(0)} = \mathbf{w}_h^n, \ \mathbf{w}_h^{(r)} = \mathbf{w}_h^{n+1}, \tag{53}$$

with r representing the order of the scheme and n is the number of time step. For a second-order TVB-RK method, the coefficients can be represented as [28,78]

$$\alpha_{10}=\gamma_{10}=1, \ \alpha_{20}=\alpha_{21}=\gamma_{21}=\frac{1}{2}, \ \gamma_{20}=d_0=0, \ d_1=1. \tag{54}$$

While, for a third-order scheme, they are expressed as

$$\alpha_{10}=\gamma_{10}=1, \ \alpha_{20}=\frac{3}{4}, \ \gamma_{20}=0, \ \alpha_{21}=\gamma_{21}=\frac{1}{4}$$

$$\alpha_{30}=\frac{1}{3}, \ \gamma_{30}=\alpha_{31}=\gamma_{31}=0, \ \alpha_{32}=\gamma_{32}=\frac{2}{3},$$

$$d_0=0, \ d_1=1, \ d_2=\frac{1}{2}. \tag{55}$$

3.1. Implementation of boundary conditions:

For a practical implementation of the boundary conditions, analogous to the Cockburn and Shu [72], position the left end of the boundary at $x_{-\frac{1}{2}}$ (i.e. $x_{-\frac{1}{2}}=0$). The Robin boundary conditions defined in Eq. (10) at the inlet are transformed for DG-FEM scheme as

$$\bar{c}_{i,-\frac{1}{2}}(t) = c_i(t, 0), \ \tilde{c}_{i,0}^{(mod)} = mm(\tilde{c}_{i,0}, \Delta_{k+}c_{i,0}^{(0)}, 2(c_{i,0}^{(0)} - c_i(t, 0))), \tag{56}$$

$$\tilde{\tilde{c}}_{i,0}^{(mod)} = mm(\tilde{c}_{i,0}, \Delta_{j+}c_{i,0}^{(0)}) \tag{57}$$

Similarly, the Neumann boundary conditions at the outlet are employed as:

$$\left.\frac{\partial c_i^{(l)}}{\partial x}\right|_{x=1} = 0. \tag{58}$$

VALIDATION OF NUMERICAL RESULTS THROUGH CONSISTENCY TEST

Chromatographic reactors still lack experimental evidence for the validation of their mathematical models. These models comprise mass and energy balance equations. Therefore, integral consistency analysis is a great mean to deal with the nonlinear behavior of the reaction dynamics and to study the validity and accuracy of the applied numerical scheme. Since a chromatographic reactor involves chemical reactions, the reaction stoichiometry plays an important role to investigate the correctness of numerically approximated solutions. It is a quantitative measure of the relationship between reactants and products which provide the information about the reactant used and the products produced during a chemical reaction. In the present analysis a reversible reaction of the type $R \rightleftharpoons P_1+P_2$ is considered; hence the integrated extent of the chemical reaction, ξ should satisfy the following relation:

$$\xi = n_{R,\,inj} - [n_{R,\,out} + n_{P_1,\,out} + n_{P_2,\,out}], \tag{59}$$

where ξ accounts for all the changes caused in the amount of reactant and products during the chemical reaction, n_j is the number of moles of *j*th component of the mixture and $n_{j,\,inj}=c_{j,\,inj}V_{inj}$ representing the amount of *j*th component in moles that is injected at the column inlet. Similarly, $n_{j,\,out}$ denotes the number of moles of *j*th component of the chemical reaction that is leaving the column and is given as

$$n_{j,\,out} = \dot{V}\int_0^{t_f} c_j(t, z)dt, \ k=R, P_1, R_2. \tag{60}$$

Moreover, for the present analysis only reactant R is injected at the column inlet; hence $n_{P_1,\,inj}=n_{P_2,\,inj}=0$. Also $V_{inj}=\dot{V}t_{inj}$ is the volume of the reactant that is injected at a volumetric flow rate $\dot{V}$ at the column inlet during time t_{inj}. Also, t_f is the final simulation time. Furthermore, ξ_j is the change in the number of moles of *j*th component of the reaction and is represented as

$$\xi_j = n_{j,\,inj} - n_{j,\,out}, \ j=R, P_1, P_2. \tag{61}$$

Their standard deviation, $\sigma_{\xi,j}$ can be calculated as

$$\sigma_{\xi,\,j} = \sqrt{\frac{\Sigma_{j=1}^{3}(\xi_j - \bar{\xi})}{3}}, \tag{62}$$

where $\bar{\xi}$ is the mean value of all the changes in number of moles for each involved component during the considered chemical reaction. An energy based evaluation of the underlying chemical and segregation process can be done with the comparison of enthalpies leaving and entering the system, which are represented symbolically by ΔH_{out} and ΔH_{inj}, respectively, and are given as

$$\Delta H_{inj} = c_f\dot{V}\int_0^{t_f}(T_{inj} - T_{ref})dt, \tag{63}$$

$$\Delta H_{out} = c_f\dot{V}\int_0^{t_f}(T(t, z=10) - T_{ref})dt. \tag{64}$$

Since for the present analysis we have considered in general $T_{inj}=T_{ref}$, hence $\Delta H_{out}=0$. Also for the case when *t* is so long that it represents the time for a complete adsorption-desorption cycle, the following can be demanded due to the nullification of the sorption effect:

$$\Delta H_{out} + (\Delta H_R)\xi = 0. \tag{65}$$

Hence Eq. (65) can be exploited as a check point for the accuracy of the obtained numerical results. However, in the course of applying any numerical scheme there are many sources due to which errors penetrate into the numerical solution of the given problem. These error sources include the process of space discretization, utilization of numerical integration, rounding off of the answers and many more. Due to the presence of these errors the R.H.S of Eq. (65) might not be exactly zero. Let ΔH_{error} represent the difference

of L.H.S of Eq. (65) from zero, i.e.,

$$\Delta H_{out}+(\Delta H_R)\xi=\Delta H_{error}, \tag{66}$$

where it is evident from above arguments that a small value of ΔH_{error} is the proof of an accurate numerical scheme. Moreover, a relative error in energy calculation is represented as

$$E_H=100\times\left|\frac{\Delta H_{error}}{\Delta H_R\xi}\right|. \tag{67}$$

NUMERICAL CASE STUDIES

In this section, the influences of various parameters on conversion and separation of the mixture in reactive chromatographic column are analyzed and the dynamic behavior of the involved chemical processes is studied. Which is governed by the fact of how the characteristic spatio-temporal patterns also known as non-linear waves evolve. In the present case, they are the thermal and concentration fronts. The main causes of non-linear wave propagation inside a fixed bed chromatographic reactor are chemical reaction and heat conduction [79]. Here in this section, several case studies are discussed with the emphasis on the coupling of concentration and thermal fronts. Moreover, in general, unless stated, the value of enthalpy of adsorption is assumed to be the same for all the components, that is, $\Delta H_{A,i}=\Delta H_A$ for i=1, 2, 3. The detail of different parameters involved in the chromatographic reactor is listed in Table 1. All the calculations were carried out with a grid of 100 mesh points.

1. Comparison of Numerical Schemes

This case study compares the performance of the DG-FEM scheme with other flux-limiting finite volume schemes available in the literature. We have considered the non-reactive, non-linear and non-isothermal, multi-component model. The column is initially equilibrated with the solvent, i.e., $c_{i,init}$=0.0 mol/l, $c_{i,inj}$=1.0 mol/l, t_{inj}=5.0 min, t_{max}=50.0 min, D_L=0.001 cm^2/min, u=1.5 cm/min, $\Delta H_{A,i}$=−20 kJ/mol, k=10 min^{-1}, $a_{1,ref}$=1.0, $a_{2,ref}$=3.0, $b_{i,ref}$=1.0 and N_t=1,000; moreover a grid of 100 mesh cell was utilized. Figs. 2(a) and 2(b) show a comparison of the numerical results for concentration and temperature at the column outlet. The solution of DG-FEM scheme at 2000 grid points is referred to as the reference solution. It is clearly depicted from the zoomed plots that the DG-FEM scheme gives the more resolved peaks for all components. In comparison to the DG-FEM scheme, the solution profiles produced by HR-FVS and the other schemes are less resolved. In addition, the first-order scheme produces a most diffusive profile. As far as the computational time for the considered grid point is concerned, the DG-FEM scheme has the maximum computational time as compared to Koren and other flux-limiting finite volume schemes. These findings lead us to the conclusion that the DG-FEM scheme may provide the most accurate and efficient solution for such models.

2. Isothermal Conditions Along with Linear Isotherm ($\Delta H_{A,i}$=0, ΔH_R=0 kJ/mol)

In this subsection, an ideal reference isothermal case is investi-

Table 1. Parameters used in the study

Parameters	Values
Column length	L=10.0 cm
Column porosity	ε=0.4
Axial dispersion coefficient	D_L=0.0001 cm^2/min
Injection time	t_{inj}=1.0 min
Final simulation time	t_{max}=80 min
Initial concentrations	$c_{i,init}$=0 mol/l
Initial temperature	T_{init}=300 K
Reference temperature	T_{ref}=300 K
Inlet concentration of component R	$c_{1,inj}$=1.0 mol/l
Inlet concentration of component P_1	$c_{2,inj}$=0.0 mol/l
Inlet concentration of component P_2	$c_{3,inj}$=0.0 mol/l
Adsorption equilibrium constant for component R	$a_{1,ref}$=1.5
Adsorption equilibrium constant for component P_1	$a_{2,ref}$=0.1
Adsorption equilibrium constant for component P_2	$a_{3,ref}$=4.0
Reference values of nonlinearity coefficient	$b_{i,ref}$=1 (i=1, 2, 3)
Specific heat for solid phase	c_e=4 J/Kcm^3
Specific heat for liquid phase	c_f=4 J/Kcm^3
Radius of the particle	R_p=0.004 cm
Heat transfer coefficient	h_p=1 W/cm^2K
Heat conductivity coefficient	λ_L=4D_L=0.0004 cm^2/min
Mass transfer coefficient	k=10 min^{-1}
Interstitial velocity	u=1 cm/min
Activation energy	E_{Act}=50.0 kJ/mol
Heterogeneous reaction rate constant	k^{het}=0.0005 min^{-1}
Reaction equilibrium constant	k_{eq}^{het}=0.5 mol/l

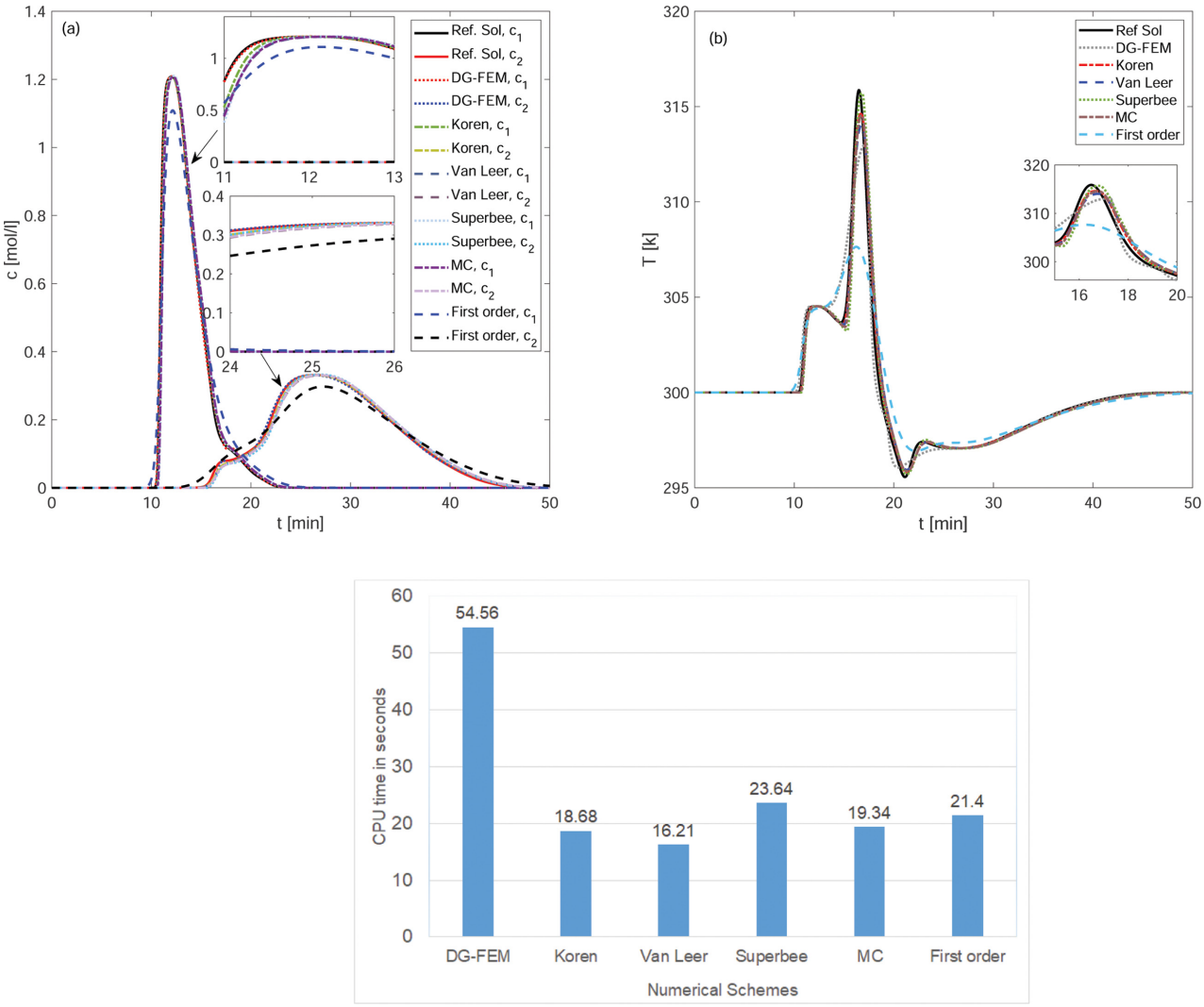

Fig. 2. A comparison of different numerical schemes and their CPU times: Concentration and temperature profiles are generated for nonlinear, non-isothermal and non-reactive multi-component model.

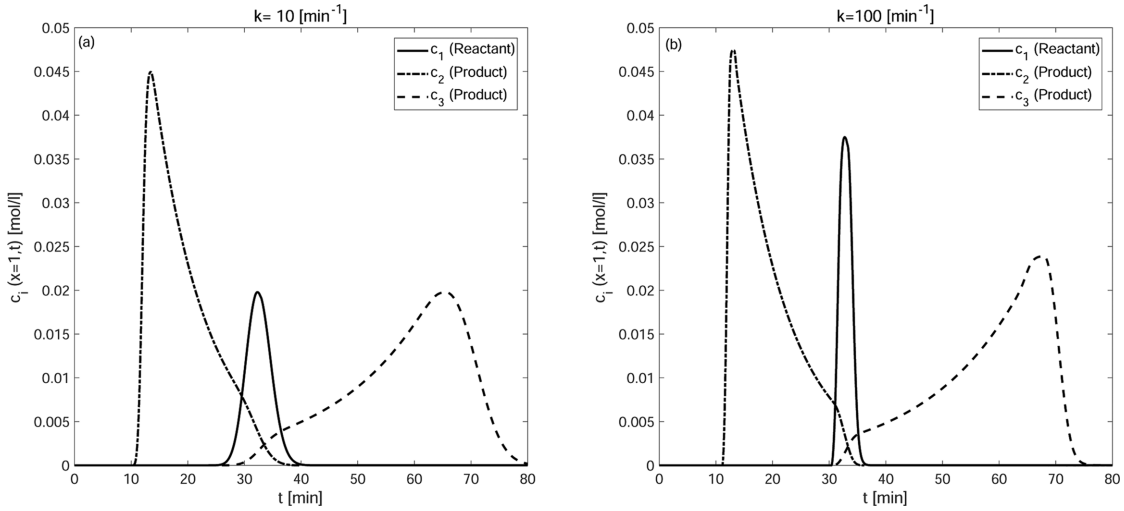

Fig. 3. Reference isothermal case for three-component reaction: Concentration profiles are generated for two different values of mass transfer coefficient k. Here $\Delta H_A=0=\Delta H_R$ kJ/mol, $b_{i,ref}=0$ for i=1, 2, 3. The values of other parameters are given in Table 1.

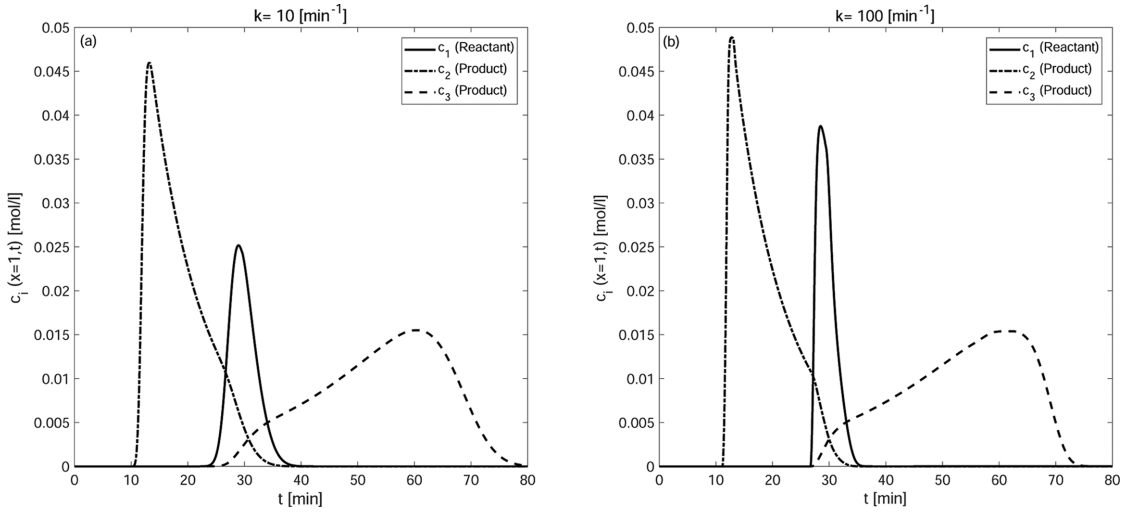

Fig. 4. Reference isothermal case for three-component reaction: Concentration profiles are generated for two different values of mass transfer coefficient k. Here $\Delta H_A=0=\Delta H_R$ kJ/mol, $b_{i,ref}=1$ for i=1, 2, 3. The values of other parameters are given in Table 1.

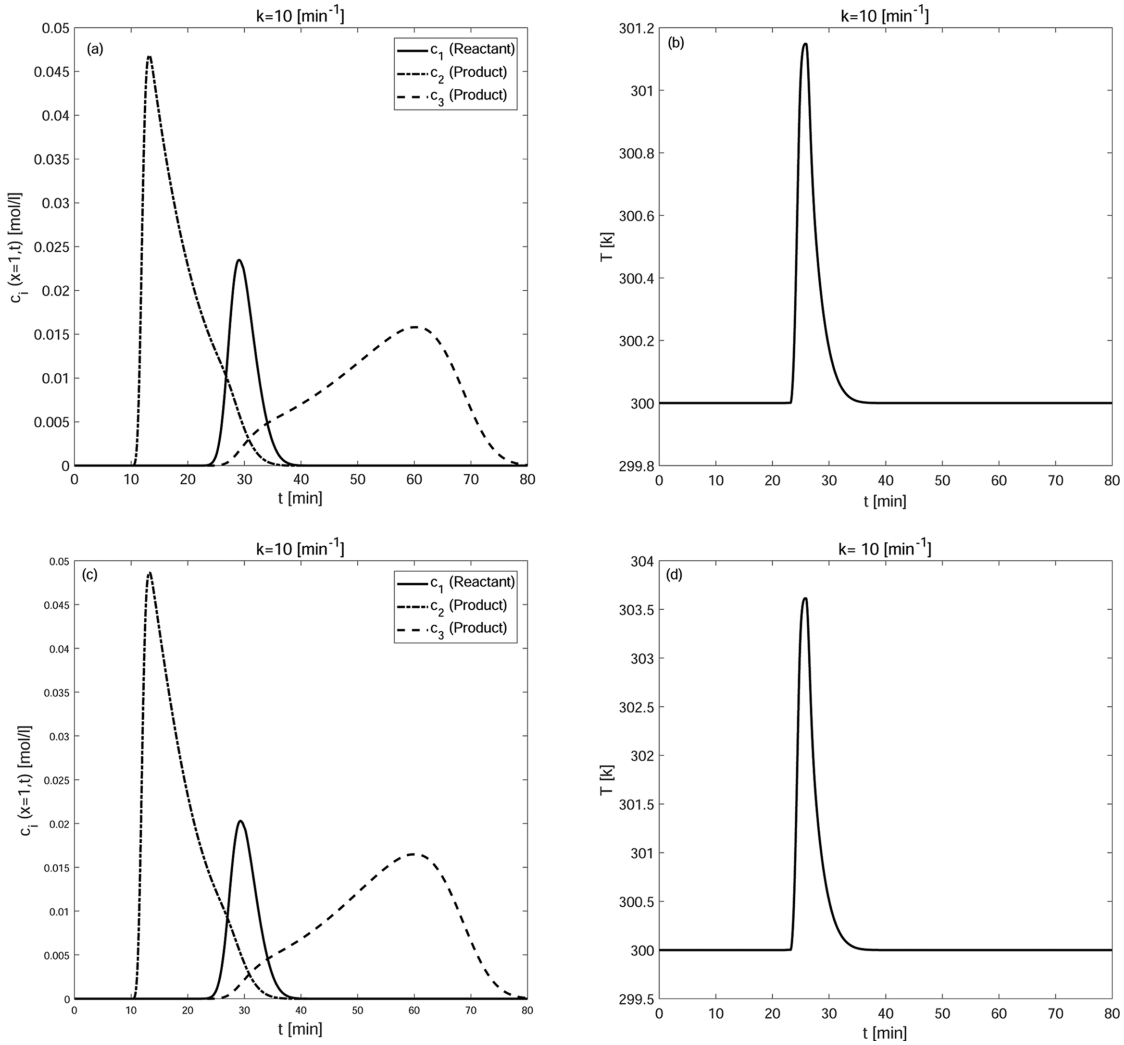

Fig. 5. Effect of enthalpy of reaction on three component reaction: Concentration and temperature profiles are generated in Figures (a) & (b) for $\Delta H_A=0$ kJ/mol $\Delta H_R=-20$ kJ/mol, $b_{i,ref}=1$ and in Figures (c) & (d) for $\Delta H_A=0$ kJ/mol $\Delta H_R=-60$ kJ/mol, $b_{i,ref}=1$ for i=1, 2, 3. The values of other parameters are given in Table 1.

gated for linear as well as nonlinear cases for two different values of the mass transfer coefficient: k=10 min^{-1}, and k=100 min^{-1}. The study helps to understand the non-isothermal case, since the reaction considered is a reversible reaction of the type $R \rightleftharpoons P_1+P_2$. Hence, only reactant is initially injected into the empty column, in the form of rectangular pulse using Danckwerts boundary condition inside the chromatographic reactor. Figs. 3 and 4 display the isothermal behavior of the process. The results depict the presence of products P_1 and P_2. The reactant is continually converted into the products owing to their different affinities towards the catalytic natured solid bed. It is further observed that the selected values of adsorption equilibrium constants give out significant but incomplete sepa-

Table 2. Results of consistency tests for varying ΔH_R, $\Delta H_{A,j}$=0 kJ/mol, k=10 min^{-1}, E_{Act}=50 kJ/mol

Parameters	ξ_R (mol)	ξ_{P_1} (mol)	ξ_{P_2} (mol)	$\sigma_{\xi,j}$ (%)	χ_R (%)	ΔH_{out} (kJ)	ΔH_{error} (kJ)	E_H (%)
ΔH_R=0	4.2779e^{-4}	2.1407e^{-4}	2.1408e^{-4}	1.0075e^{-4}	86	0	0	-
ΔH_R=−20	4.3201e^{-4}	2.1618e^{-4}	2.1617e^{-4}	1.0174e^{-4}	87	0.0086	0.0028	1.9971
ΔH_R=−60	4.4024e^{-4}	2.2030e^{-4}	2.2026e^{-4}	1.0369e^{-4}	88	0.0264	0.0088	1.9969

Table 3. Results of consistency tests for varying ΔH_A, ΔH_R=0 kJ/mol, k=10 min^{-1}, E_{Act}=50 kJ/mol

Parameters	ξ_R (mol)	ξ_{P_1} (mol)	ξ_{P_2} (mol)	$\sigma_{\xi,j}$ (%)	χ_R (%)	ΔH_{out} (kJ)	ΔH_{error} (kJ)	E_H (%)
ΔH_A=0	4.2779e^{-4}	2.1407e^{-4}	2.1408e^{-4}	1.0075e^{-4}	86	0	0	-
ΔH_A=−20	4.2984e^{-4}	2.1509e^{-4}	2.1511e^{-4}	1.0123	86	8.9543e^{-7}	8.9543e^{-7}	0
ΔH_A=−60	4.3272e^{-4}	2.1655e^{-4}	2.1651e^{-4}	1.0192	87	5.4188e^{-6}	5.4188e^{-6}	0

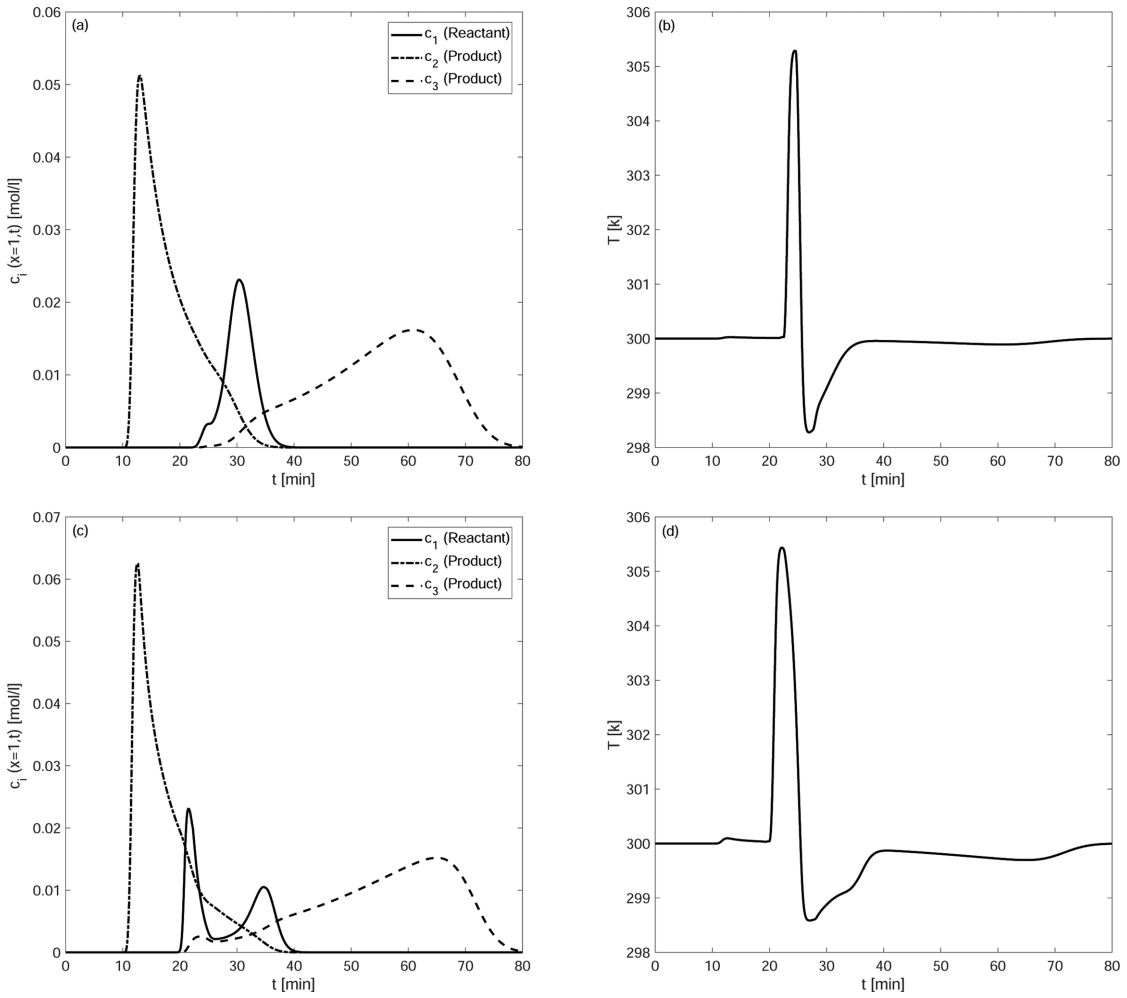

Fig. 6. Effect of enthalpy of adsorption on three component reaction: Concentration and temperature profiles are generated in Figures (a) & (b) for ΔH_A=−20 kJ/mol ΔH_R=0 kJ/mol, $b_{i,ref}$=1 and in Figures (c) & (d) for ΔH_A=−60 kJ/mol ΔH_R=0 kJ/mol, $b_{i,ref}$=1 for i=1, 2, 3. The values of other parameters are given in Table 1.

ration and conversion which is improved with an increase in the value of mass transfer coefficient, k. As expected in isothermal operating conditions, no variations are identified in the temperature profile.

3. Effects of Enthalpy of Reaction ($\Delta H_{A,i}$=0 kJ/mol, $\Delta H_R \neq 0$ kJ/mol)

The effect of enthalpy of reaction (ΔH_R) in the case of an exothermic reaction is analyzed in this subsection for two different values of ΔH_R i.e. −20 kJ/mol, −60 kJ/mol. Fig. 5 accounts for variations in concentration and temperature fronts for different values of enthalpy of reaction. It can be observed that the temperature fronts display a single smooth peak in contrast to the isothermal case where no temperature changes are noticed. The observed single peak accounts for the exothermicity of the reaction. Moreover, temperature fronts peak enlarged as a consequence of increase in enthalpy of reaction, which in turn resulted in an improved conversion of reactant into products (c.f. Table 2). The rate of conversion is 87% for ΔH_R=−20 kJ/mol, which further improves to 88% for ΔH_R=−60 kJ/mol. Furthermore, the non-linearity effects are more significant for larger values of enthalpy of reaction.

4. Effects of Enthalpy of Adsorption ($\Delta H_{A,i} \neq 0$ kJ/mol, ΔH_R= 0 kJ/mol)

The present case study quantifies the effect of enthalpy of adsorption ($\Delta H_{A,i}$) for the case when enthalpy of reaction is negligible: (ΔH_R=0 kJ/mol). The enthalpies of adsorption play an important role in the separation of reactant and products because segregation is a consequence of differences in the level of adsorption of different components to the stationary phase which is highly dependent on temperature fluctuations, which in turn mostly result from the change in enthalpy of adsorption. Hence, choosing a larger value of enthalpy of adsorption is expected to be accompanied by more retention time, sharpness of thermal especially concentration fronts, and relatively less conversion and segregation (c.f. Table 3). These effects are depicted in Fig. 6.

5. Combined Effects of Enthalpies of Reaction and Adsorption ($\Delta H_R \neq 0$ kJ/mol, $\Delta H_{A,i} \neq 0$ kJ/mol)

For a comprehensive analysis of a non-isothermal chromato-

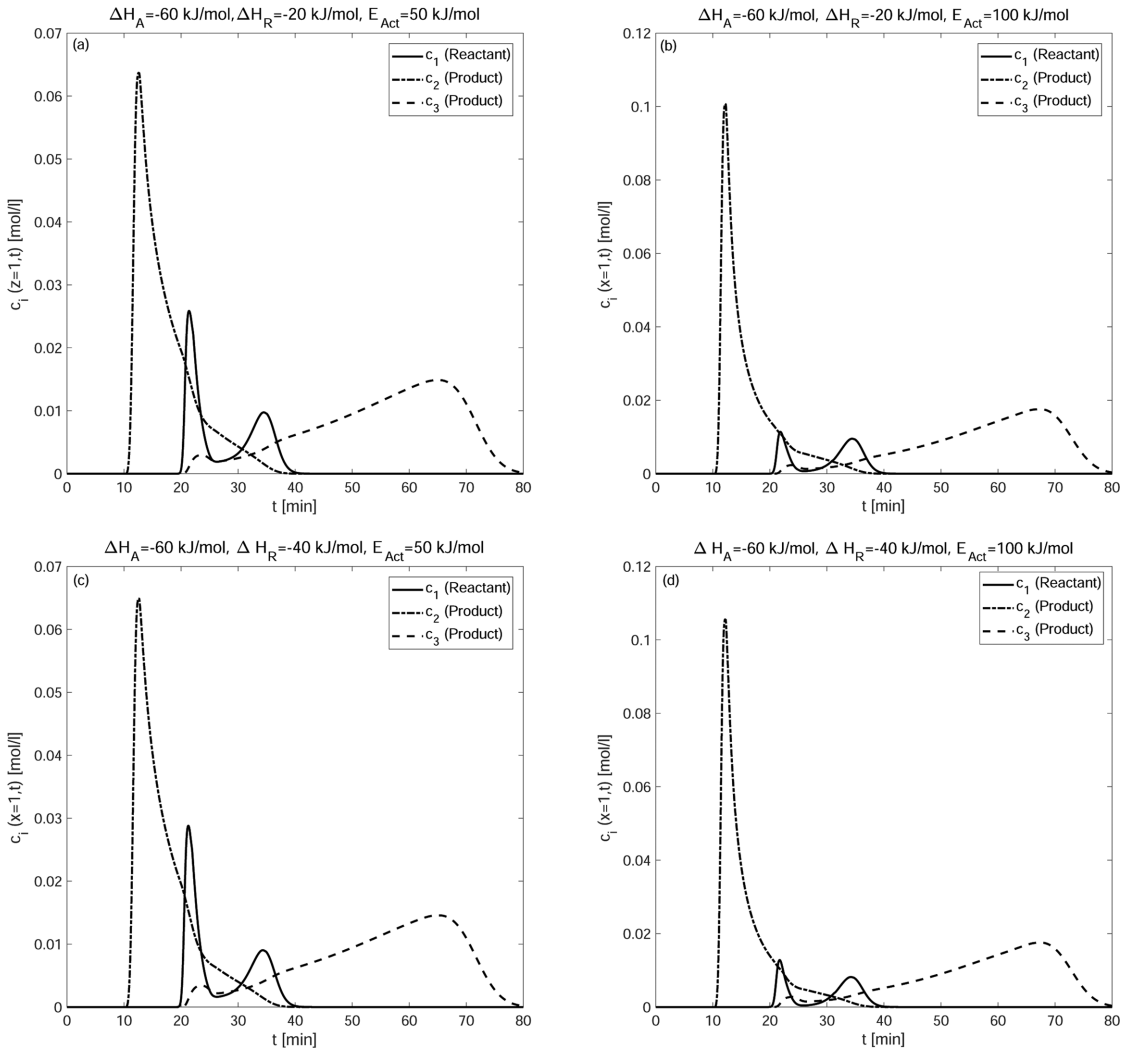

Fig. 7. Combined effects of enthalpy of adsorption, enthalpy of reaction, and activation energy on three component reaction: Concentration profiles are generated in Figures (a) & (c) for ΔH_A=−60 kJ/mol ΔH_R=−20 kJ/mol E_{Act}=50 kJ/mol, $b_{i,ref}$=1 and in Figures (b) & (d) for ΔH_A=−60 kJ/mol ΔH_R=−40 kJ/mol E_{Act}=100 kJ/mol, $b_{i,ref}$=1 for i=1, 2, 3. The values of other parameters are given in Table 1.

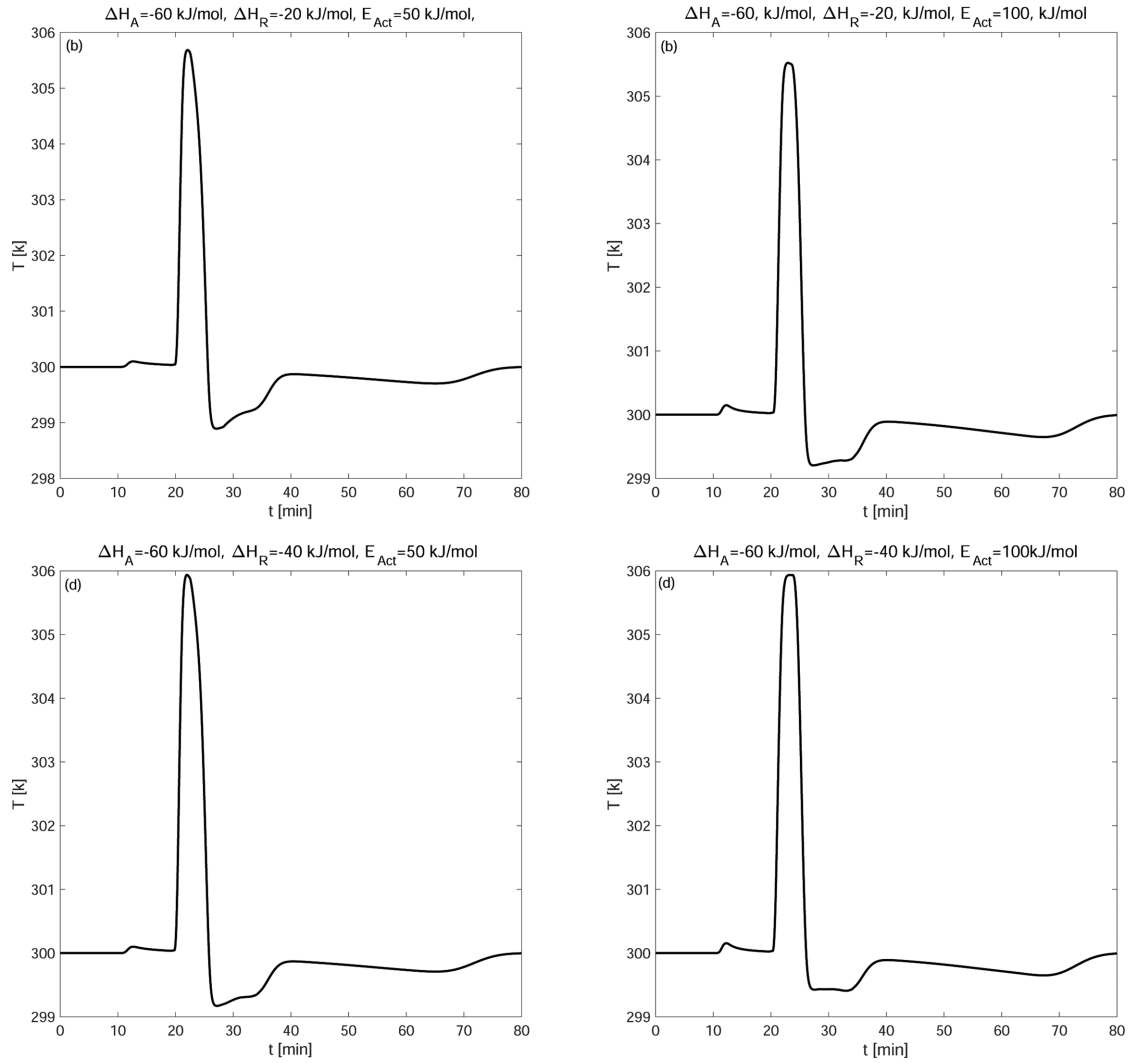

Fig. 8. Combined effects of enthalpy of adsorption, enthalpy of reaction, and activation energy on temperature during the three component reaction: Temperature profiles are generated in Figures (a) & (c) for ΔH_A=−60 kJ/mol ΔH_R=−20 kJ/mol E_{Act}=50 kJ/mol, $b_{i,ref}$=1 and in Figures (b) & (d) for ΔH_A=−60 kJ/mol ΔH_R=−40 kJ/mol E_{Act}=100 kJ/mol, $b_{i,ref}$=1 for i=1, 2, 3. The values of other parameters are given in Table 1.

Table 4. Performance evaluation for the combined effects of enthalpies of reaction and adsorption $\Delta H_{A,j}$=−60 kJ/mol, ΔH_R=−20 kJ/mol, k=10 min^{-1}

Parameters	ξ_R (mol)	ξ_{P_1} (mol)	ξ_{P_2} (mol)	$\sigma_{\xi,j}$ (%)	χ_R (%)	ΔH_{out} (kJ)	ΔH_{error} (kJ)	E_H (%)
E_{Act}=50	$4.3238e^{-4}$	$2.1638e^{-4}$	$2.1633e^{-4}$	$1.0184e^{-4}$	87	0.0087	0.0029	1.9921
E_{Act}=100	$4.5779e^{-4}$	$2.2908e^{-4}$	$2.2892e^{-4}$	$1.0785e^{-4}$	92	0.0092	0.0031	1.9861

Table 5. Performance evaluation for the combined effects of enthalpies of reaction and adsorption $\Delta H_{A,j}$=−60 kJ/mol, ΔH_R=−40 kJ/mol, k=10 min^{-1}

Parameters	ξ_R (mol)	ξ_{P_1} (mol)	ξ_{P_2} (mol)	$\sigma_{\xi,j}$ (%)	χ_R (%)	ΔH_{out} (kJ)	ΔH_{error} (kJ)	E_H (%)
E_{Act}=50	$4.3202e^{-4}$	$2.1620e^{-4}$	$2.1614e^{-4}$	$1.0175e^{-4}$	87	0.0173	0.0058	1.9946
E_{Act}=100	$4.6148e^{-4}$	$2.3093e^{-4}$	$2.3075e^{-4}$	$1.0872e^{-4}$	93	0.0185	0.0062	1.9910

graphic reactor, effects of the enthalpies of adsorption, reaction and activation energy are considered simultaneously (c.f. Figs. 7 and 8). As is evident from the previous case studies that an increase in the value of enthalpy of reaction, ΔH_R, results in larger temperature profile peaks which help to improve conversion of the reactant into products. Also, enthalpy of adsorption affects the extent of adsorp-

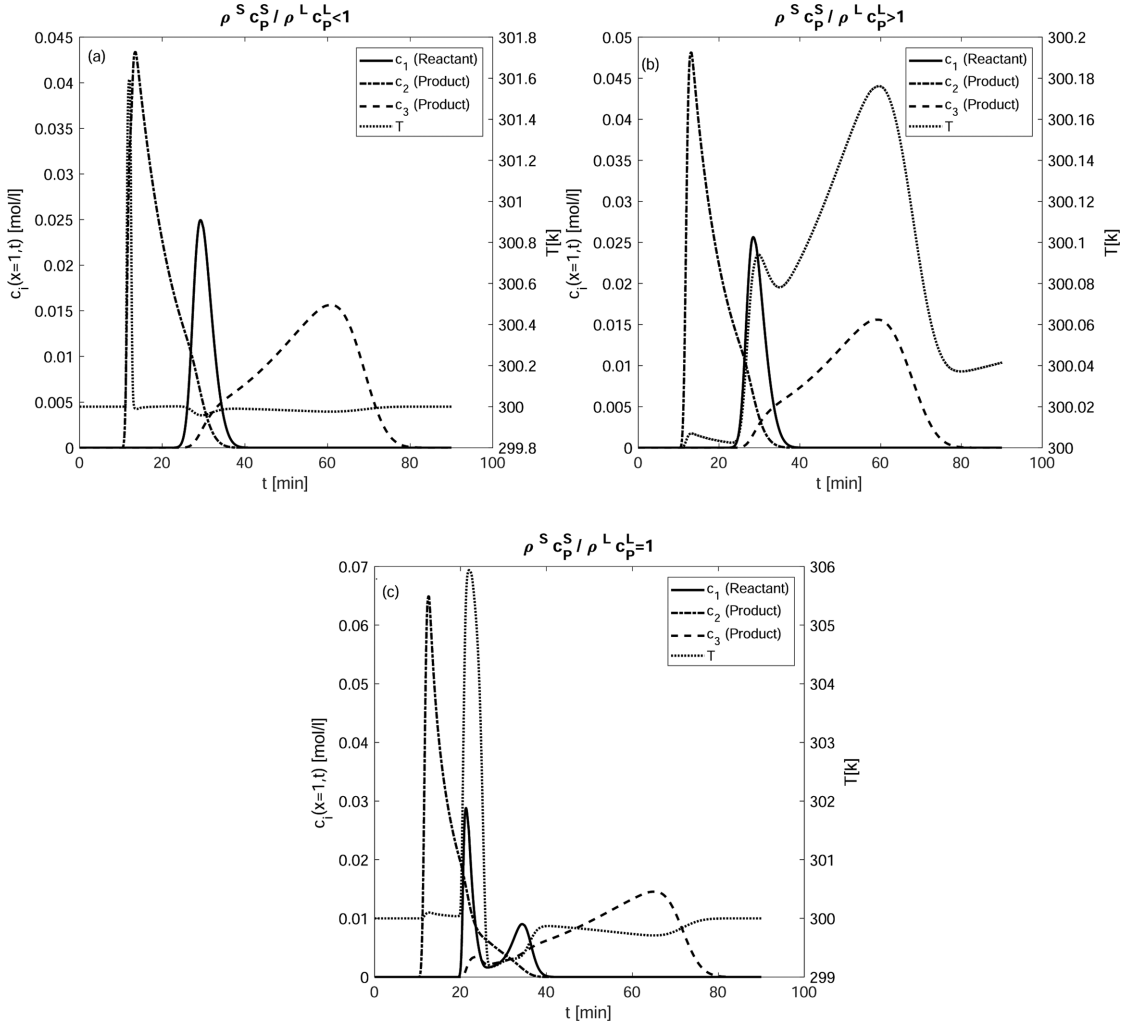

Fig. 9. Effects of the ratio c_e/c_f: Concentration and temperature profiles are generated in Figures (a) & (b) for ΔH_A=−60 kJ/mol ΔH_R=−40 kJ/mol, $b_{i,ref}$=1 and in Figures (c) & (d) for ΔH_A=−60 kJ/mol ΔH_R=−40 kJ/mol, $b_{i,ref}$=1, c_e=40 J/Kcm^3, c_f=4 J/Kcm^3 for i=1, 2, 3. The values of other parameters are given in Table 1.

tion; hence an increased value of enthalpy of adsorption means less retention time. Furthermore, activation energy and conversion are directly proportional to each other. So when the value of activation energy increases, more reactant is converted into products as illustrated by Tables 4 and 5. Here by increasing the value of activation energy from 50 kJ/mol to 100 kJ/mol, the percentage conversion of reactant into product has improved from 87% to 92% for the case when $\Delta H_{A,j}$ = −60 kJ/mol and ΔH_R=−20 kJ/mol. And improved further from 87% to 93% for the case when $\Delta H_{A,j}$=−60 kJ/mol and ΔH_R=−40 kJ/mol. Thus, large values of activation energy enhances the reaction rate. The corresponding quantitative values given in Tables 4 and 5 demonstrate the precision of numerical solutions.

6. Effects of Ratio $\frac{c_e}{c_f}$

Fig. 9 portrays the influence caused by changing the ratio $\frac{\rho^S c^S}{\rho^L c^L}$ on both concentration and energy profiles. For the present analysis, we considered $\Delta H_{A,i}$=−60 kJ/mol, ΔH_R=−40 kJ/mol and E_{Act}= 50 kJ/mol. It can be seen through Fig. 9((a), (b), and (c)) that the ratio $\frac{\rho^S c^S}{\rho^L c^L}$ influences the propagation speed of both concentration and temperature wave fronts. When $\frac{\rho^S c^S}{\rho^L c^L}$=0.1<1 the energy wave front is moving at the fastest speed in comparison to the three concentration fronts; moreover, the adsorption peek is much higher than the desorption peak. A decoupling between reactant and energy wave fronts can also be seen in Fig. 9(a). Whereas when $\frac{\rho^S c^S}{\rho^L c^L}$=4>1 (c.f. Fig. 9(b)) the energy profile has three adsorption peaks, each coupled with one of the three concentration profiles, resulting in the largest percentage conversion of reactant into products. When $\frac{\rho^S c^S}{\rho^L c^L}$=1, the energy profile has the largest adsorption peak and is coupled to the reactant profile. Hence, it can be concluded that the ratio $\frac{\rho^S c^S}{\rho^L c^L}$ has significant influence on the speed of the temperature profile and conversion of reactant into products.

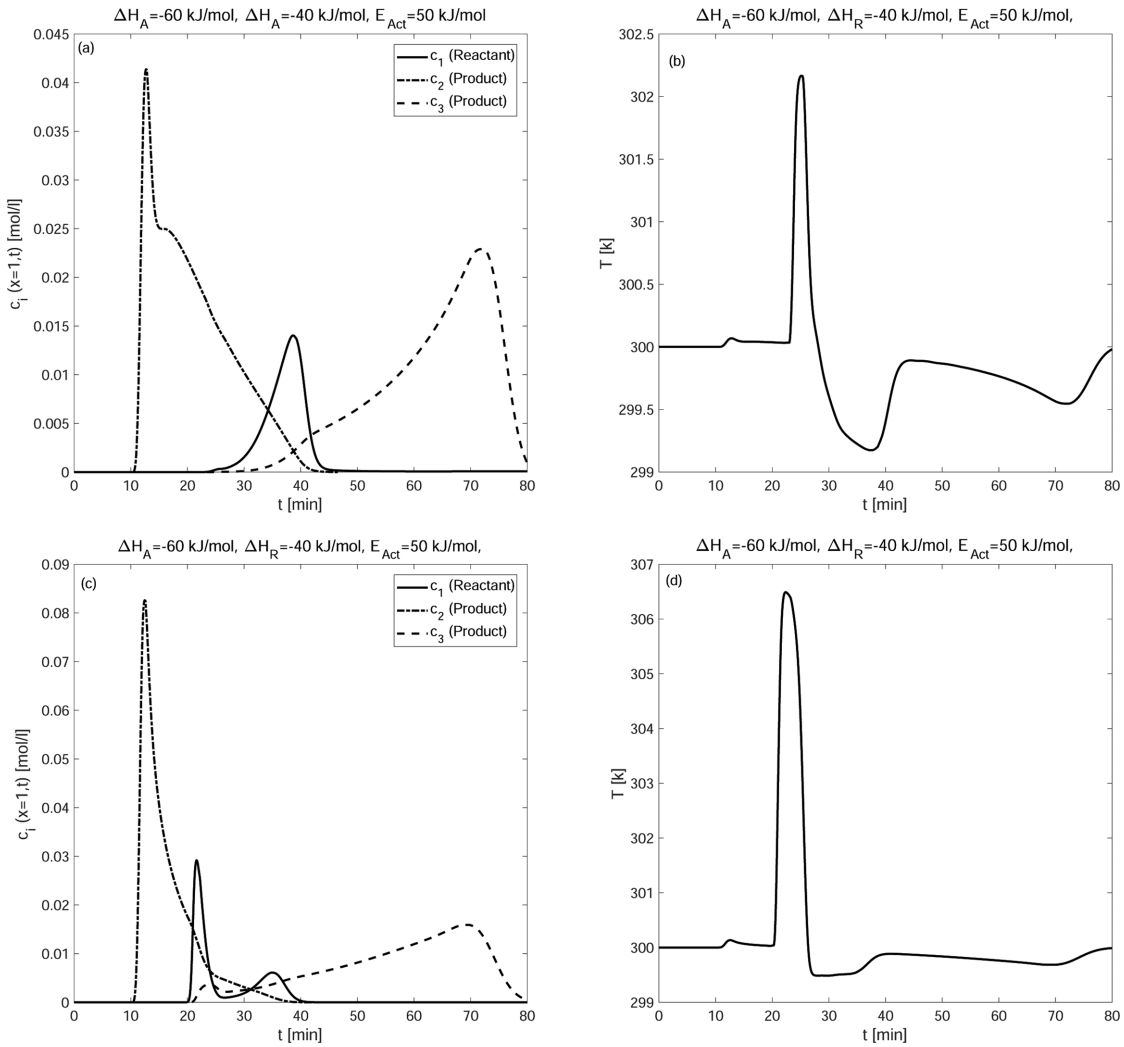

Fig. 10. Effects of cold ((a) & (b)) and hot ((c) & (d)) injections on concentration and temperature profiles during the three-component reaction: Concentration and temperature profiles are generated for ΔH_A=−60 kJ/mol, ΔH_R=−40 kJ/mol, E_{Act}=50 kJ/mol, $b_{i,ref}$=1 for i=1, 2, 3. The values of other parameters are given in Table 1.

7. Effects of Injected Temperature ($T_{inj} \neq T_{ref}$)

Fig. 10 displays the results of the scenario when the temperature of the injected sample, T_{inj}, is not same as that of the mobile phase temperature, T_{ref}. For the present study two obvious cases, cold injection and hot injection, are discussed. For this purpose, we have considered T_{inj}=280 K and 305 K instead of being equal to the reference temperature whose value is taken to be 300 K. It can be observed through Figs. 10((a), (b), (c), and (d)) that many considerable changes can be seen for differing temperature of the injected sample from that of the reference temperature. First, the noticeable and obvious change in the case of hot injection is the increase in adsorption peak and decrease in desorption peak of the temperature profile when compared to the temperature profile for the case of cold injection. Also, due to the hot injection, conversion has improved and retention time has decreased in comparison to the cold injection case. Hence, hot injection increases the conversion process, decreases retention time, resulting in an improvement of the overall performance of the chromatographic reactor.

CONCLUSION

A nonlinear, non-isothermal, and reactive (RLKM) was formulated and approximated numerically. The analysis focused on the reaction of the type $R \rightleftharpoons P_1+P_2$, where a single component was injected inside the column in the form of a rectangular pulse, and due to the catalytic nature of the stationary phase, products P_1 and P_2 were produced. The resulting mass and energy balance system consists of convection diffusion reaction PDEs, coupled with algebraic and differential equations for adsorption isotherm and reaction kinetics. In the light of this complexity, the Runge-Kutta discontinuous Galerkin finite element method was proposed to gain the numerical solution of the model equations. As chromatographic reactors still lack experimental evidence for validation of their mathematical models; therefore, integral consistency analysis was introduced for verifying the validity and accuracy of the applied numerical scheme. The analysis reveals that there are many important factors, each influencing the performance of the reactor. These fac-

tors include the enthalpy of adsorption, the enthalpy of reaction, the difference between the temperature of the injected sample and reference temperature, the ratio $\frac{c_e}{c_f}$, and the mass transfer coefficients k. The study concluded that enthalpy of reaction and adsorption have direct influence on the performance of the reactor, as an increased value of enthalpy of reaction produces much higher temperature fronts, while enthalpy of adsorption is directly proportional to the extent of adsorption. It was also noticed that the ratio $\frac{c_e}{c_f}$ affects the propagation speed of energy and mass profiles, and maximum conversion was observed for the case when $\frac{c_e}{c_f}>1$. Hence, it can be concluded that a detailed study of the above mentioned parameters is essential to enhance reactor performance.

REFERENCES

1. B. R. Bhandare, *AJChE*, **7**(1), 1 (2019).
2. A. E. Rodrigues, C. S. M. Pereira and C. S. M. Santos, *Chem. Eng. Technol.*, **35**, 1171 (2012).
3. M. Kawase, T. B. Suzuki, K, Inoue, K. Yoshimoto and K. Hashimoto, *Chem. Eng. Sci.*, **51**, 2971 (1996).
4. J. Schmidt, D. Reusch, K. Elgeti and R. Schomcker, *Chem. Ingenieur Technik*, **71**(7), 704 (1999).
5. M. Kawase, Y. Inoue, T. Araki and K. Hashimoto, *Catal. Today*, **48**(1-4), 199 (1999).
6. M. T. Shieh and P. E. Barker, *J. Chem. Technol. Biotechnol.*, **66**(3), 265 (1996).
7. A. Howard, G. Carta and C. Byers, *Ind. Eng. Chem. Res.*, **27**, 1873 (1988).
8. A. K. Ray and R. W. Carr, *Chem. Eng. Sci.*, **50**(14), 2195 (1995).
9. S. Gruner and A. Kienle, *Chem. Eng. Sci.*, **59**(4), 901 (2004).
10. T. D. Vu, A. Seidel-Morgenstern, S. Gruner and A. Kienle, *Ind. Eng. Chem. Res.*, **44**, 9565 (2005).
11. A. Brandt, G. Mann and W. Arlt, *J. Chromatogr. A.*, **769**(1), 109 (1997).
12. E. Lundanes and T. Greibrokk, *Adv. Chromatogr.*, **44**, 45 (2006).
13. T. Sainio, Ion-exchange resins as stationary phase in reactive chromatography. Acta Universitatis Lappeenrantaensis 218, Diss. Lappeenranta University of Technology, Finland (2005).
14. T. Sainio, M. Kaspereit, A. Kienle and A. Seidel-Morgenstern, *Chem. Eng. Sci.*, **62**, 5674 (2007).
15. T. Sainio, L. Zhang and A. Seidel-Morgenstern, *Chem. Eng. J.*, **168**, 861 (2011).
16. S. Qamar, F. A. Sattar and A. Seidel-Morgenstern, *Chem. Eng. Res. Des.*, **115**, 145 (2016).
17. K. Kaczmarski, F. Gritti and G. Guiochon, *J. Chromatogr. A.*, **1177**(1), 92 (1969).
18. R. L. Cerro and W. Smith, *Ind. Eng. Chem. Fund.*, **8**, 796 (1969).
19. J. W. Dolan, *J. Chromatogr. A.*, **965**, 195 (2002).
20. T. Greibrokk and T. Andersen, *J. Chromatogr. A.*, **1000**, 743 (2003).
21. L. C. Sander and S. A. Wise, *J. Sep. Sci.*, **24**, 910 (2001).
22. H. Go, Y. Sudo, T. Hosoya, T. Ikegami and N. Tanaka, *Anal. Chem.*, **70**, 4086 (1998).
23. K. Kurata, T. Shimoyama and A. Dobashi, *J. Chromatogr. A.*, **1012**, 47 (2003).
24. F. D. Antia and C. Horvath, *J. Chromatogr. A.*, **435**, 1 (2008).
25. H. W. Haynes Jr., *AIChE J.*, **32**, 1750 (1986).
26. G. M. Zhong and F. Meunier, *J. Chromatogr. A.*, **658**, 355 (1994).
27. T. D. Vu and A. Seidel-Morgenstern, *J. Chromatogr. A.*, **1218**, 8097 (2011).
28. S. Javeed, S. Qamar, A. Seidel-Morgenstern and G. Warnecke, *J. Chromatogr. A.*, **1218**(40), 7137 (2016).
29. T. Andersen, M. Pepaj, R. Trones, E. Lundanes and T. Greibrokk, *J. Chromatogr. A.*, **1025**, 217 (2004).
30. M. Busch and A. Seubert, *Anal. Chim. Acta*, **399**, 223 (1999).
31. Y.-X. Song, J.-Q. Wang, Z.-X. Su and D.-Y. Chen, *Chromatographia*, **54**, 208 (2001).
32. G. Carta, *Chem. Eng. Sci.*, **43**, 2877 (1988).
33. D. M. Ruthven, *Principles of adsorption and adsorption processes*, Wiley-Interscience, New York (1984).
34. G. Guiochon and B. Lin, *Modeling for preparative chromatography*, Elsevier Academic Press (2003).
35. A. Felinger, A. Cavazzini and F. Dondi, *J. Chromatogr. A.*, **1043**(2), 149 (2004).
36. G. Guiochon, A. Felinger, D. G. Shirazi and A. M. Katti, *Fundamentals of preparative and nonlinear chromatography*, 2nd ed; Elsevier Academic Press: New York (2006).
37. S. Qamar, S. Perveen and A. Seidel-Morgenstern, *Ind. Eng. Chem. Res.*, **55**, 9003 (2016).
38. S. Qamar, D. U. Uche, F. U. Khan and A. Seidel-Morgenstern, *J. Chromatogr. A.*, **1496**, 92 (2017).
39. C. W. Shu and S. Osher, *J. Comput. Phys.*, **77**(2), 439 (1988).
40. A. Harten, B. Engquist, S. Osher and S. R. Chakravarthy, *J. Comput. Phys.*, **71**(2), 231 (1987).
41. K. W. Morton and P. K. Sweby, *J. Comput. Phys.*, **73**(1), 203 (1987).
42. A. Harten, *SIAM J. Numer. Anal.*, **21**(1), 1 (1984).
43. A. Harten, Preliminary results on the extension of ENO schemes to two-dimensional problems. In: Carasso C., Serre D., Raviart PA. (eds) Nonlinear hyperbolic problems. Lecture Notes in Mathematics Springer, Berlin, Heidelberg 1270 (1987).
44. A. Harten and S. Osher, *SIAM J. Numer. Anal.*, **24**(2), 279 (1985).
45. S. Osher, *SIAM J. Numer. Anal.*, **22**(5), 947 (1985).
46. S. Osher and S. Chakravarthy, *SIAM J. Numer. Anal.*, **21**(5), 955 (1984).
47. S. Osher and E. Tadmor, *Math. Comput.*, **50**(181), 19 (1988).
48. R. Sanders, *Math. Comput.*, **51**(184), 535 (1988).
49. C. W. Shu, *Math. Comput.*, **49**(179), 105 (1987).
50. C. W. Shu, *Math. Comput.*, **49**(179), 123 (1987).
51. C. W. Shu, *SIAM J. Sci. Stat. Comput.*, **9**(6), 1073 (1988).
52. C. Shu, *J. Comput. Phys.*, **83**, 439 (1989).
53. S. Javeed, S. Qamar, A. Seidel-Morgenstern and G. Warnecke, *J. Comput. Chem. Eng.*, **35**, 2294 (2011).
54. B. Medi and M. Amanullah, *Ind. Eng. Chem. Res.*, **50**(3), 1739 (2011).
55. S. Javeed, S. Qamar, W. Ashraf, A. Seidel-Morgenstern and G. Warnecke, *Chem. Eng. Sci.*, **90**, 17 (2013).
56. P. K. Sweby, *SIAM J. Numer. Anal.*, **21**(5), 995 (1984).
57. B. A. Koren, Robust upwind discretization method for advection, diffusion and source terms. Amsterdam: Centrum voor Wiskunde en Informatica (1993).
58. E. V. Lieres and J. Andersson, *J. Comput. Chem. Eng.*, **34**, 1180

(2010).
59. X.-D. Liu, S. Osher and T. Chan, *J. Comput. Phys.*, **115**(1), 200 (1994).
60. G.-S. Jiang and C. W. Shu, *J. Comput. Phys.*, **126**(1), 202 (1996).
61. C. W. Shu and S. Osher, *J. Comput. Phys.*, **77**(3), 439 (1988).
62. Y.-i. Lim, S.-C. Chang and S. B. Jrgensen, *Comput. Chem. Eng.*, **28**(8), 1309 (2004).
63. O. Shipilova, T. Sainio and H. Haario, *J. Chromatogr. A.*, **1204**(1), 62 (2008).
64. S. Javeed, S. Qamar, A. Seidel-Morgenstern and G. Warnecke, *J. Chroma. A.*, **1218**, 7137 (2011).
65. K. Meyer, J. K. Huusom and J. Abildskov, *Comput. Chem. Eng.*, **124**, 172 (2019).
66. A. Hrsholt, L. H. Christiansen, K. Meyer, J. K. Huusom and J. B. Jrgensen, *IFAC PapersOnLine*, **52**(1), 346 (2019).
67. A. Khan, S. Perveen and S. Qamar, *J. Liq. Chromatogr. Relat. Technol.*, **44**(5-6), 298 (2021).
68. S. Zafar, S. Perveen and S. Qamar, *J. Liq. Chromatogr. Relat. Technol.*, **44**(1-2), 52 (2021).
69. A. Khan, S. Perveen and S. Qamar, *Ind. Eng. Chem. Res.*, **60**(34), 12592 (2021).
70. W. Li and N. Zabaras, *Comput. Mater. Sci.*, **44**(4), 1163 (2009).
71. S. Qamar, I, Hussain and A. Seidel-Morgenstern, *Ind. Eng. Chem. Res.*, **50**(7), 4113 (2011).
72. B. Cockburn and C. W. Shu, *Math. Comput.*, **52**(186), 411 (1989).
73. P. Zhang and R. X. Liu, *J. Comput. Appl. Math.*, **176**(1), 105 (2005).
74. R. J. LeVeque, Finite volume methods for hyperbolic problems (Vol. 31). Cambridge university press (2002).
75. A. Kurganov and E. Tadmor, *J. Comput. Phys.*, **160**(1), 241 (2000).
76. G. S. Jiang and C. W. Shu, *Math. Comput.*, **62**(206), 531 (1994).
77. C. Johnson, *SIAM J. Numer. Anal.*, **25**(4), 908 (1988).
78. B. Cockburn and C. W. Shu, *J. Sci. Computing*, **16**(3), 173 (2001).
79. S. Gruner and A. Kienle, *Chem. Eng. Sci.*, **59**(4), 901 (2004).